An Introduction to Magnetic Fields in Neutron Stars

Luciano Rezzolla*

SISSA, International School for Advanced Studies and INFN, Trieste, Italy

Department of Physics and Astronomy, Louisiana State University, Baton Rouge, LA 70803 USA

Lectures given at the Advanced School of the 7th SFB Transregio on:

"Structure and Dynamics of Compact Objects", Albert Einstein Institute, September 20–25 2004, Golm, Germany

*www.sissa.it/∼rezzolla

1 Introduction

These lectures are aimed at introducing the properties of magnetized neutron stars (NSs) and the impact that MFs have on the structure, stability, and observability of NSs via electromagnetic (EM) or gravitational radiation. This a very vast field of research, partly penalised by the complexity that any physical acquires every time a magnetic field is present and partly by the difficulty to determine general behaviours as these are very sensitive on the specific conditions under which the system is considered.

As a result, what discussed in these lectures will serve only as a first step to a more detailed study which can be found in the references reported here. In this framework I will try and give a brief but as much as possible complete picture of the relevance of magnetic fields in NSs, discussing the observational evidence of their existence, their possible gener-

ation in proto neutron stars (PNSs) via dynamo actions, their impact on the structure and stability of NSs stars, finally considering their evolution and the processes through which they could produce intense emission of EM or gravitational waves (GWs).

A brief summary of the main topics covered is listed below and while I will not probably mention all of them, the interested reader can find here a first sketchy introduction.

- *Observational evidence of intense MFs in NSs*
- *A brief introduction to the MHD equations*
- *Generation of MFs in PNSs and NSs*
- *Structure and stability of magnetized NSs*
- *General relativistic electrodynamics of NSs*
- *Gravitational radiation from magnetized NSs*
- *MF evolution in rotating and cooling NSs*

2 Observational Evidence

The observational evidence of intense magnetic fields threading NSs comes essentially in two different forms. The first one is in the spectra of some X-ray pulsars which either show absorption features associated to a very strong MF (e.g. 1E 1207.4-5209, Sanwal et al. 2002) or in emission lines that could be interpreted cyclotron emission lines from a corona above the pulsar's polar cap (e.g. PSR B1821-24, Becker et al. 2002). The second observational evidence is now very well established and accurate as it comes from the observations of radio pulsars. These objects were first detected in 1967 (Hewish et al. 1968) and soon after their discovery it was proposed that they were rotating NSs with MF of around 10^{12} G, loosing rotational energy through dipolar EM radiation and progressively spinning down (Pacini 1967, Gold 1968).

2.1 The Rotating Dipole Model

A model that accounts for many of the observational properties of pulsars is the rotating dipole model, in which the NS is assumed to be a perfectly conducting sphere of radius R rotating in *vacuum* at an angular velocity Ω. Furthermore, it possesses a magnetic dipole moment $\boldsymbol{\mu}$ which is inclined at an angle χ with respect to $\boldsymbol{\Omega}$, i.e. $\chi = \cos^{-1}(\boldsymbol{\Omega} \cdot \boldsymbol{\mu})$. The purely dipolar MF at the stellar pole B_p is then related to the magnetic moment as

$$|\boldsymbol{\mu}| = \frac{B_\mathrm{p} R^3}{2} \,. \tag{1}$$

The whole system will have a time-varying dipole as seen from infinity and thus emit EM radiation at a rate

$$\left(\frac{dE}{dt}\right)_\mathrm{EM} = -\frac{2}{3c^3}\left(\frac{d^2|\boldsymbol{\mu}|}{dt^2}\right)^2 \,. \tag{2}$$

If $\mathbf{e}_{\parallel}, \mathbf{e}_{\perp}$ and $\mathbf{e}'_{\perp}$ are the unit vectors parallel and orthogonal to $\mathbf{\Omega}$, we can decompose the magnetic moment as

$$\boldsymbol{\mu} = \frac{B_{\rm p} R^3}{2} \left(\mathbf{e}_{\parallel} \cos\chi + \mathbf{e}_{\perp} \sin\chi \cos\Omega t + \mathbf{e}'_{\perp} \sin\chi \sin\Omega t \right) \ , \tag{3}$$

and the rate of energy-loss can be expressed explicitely as

$$\frac{dE_{\rm EM}}{dt} = \frac{\Omega^4 R^6 B_0^2}{6c^3} \sin^2\chi = I\Omega \frac{d\Omega}{dt} \ , \tag{4}$$

where the last equality in (4) assumes that the EM losses are tapping energy from the rotational kinetic one $E_{\rm rot} = I\Omega^2/2$, where I is the moment of inertia.

Defining the characteristic age at present time as $T \equiv (\Omega/\dot{\Omega})_0$, we can integrate the expression for the energy-loss rate (4) to obtain the pulsar spin evolution

$$\Omega(t) = \Omega_{\rm i} \left(1 + \frac{2\Omega_{\rm i}^2}{\Omega_0^2} \frac{t}{T} \right)^{-1/2} \ , \tag{5}$$

where $\Omega_{\rm i}$ is the initial spin, Ω_0 the present one and the pulsar's present age is $t \approx T/2$ if $\Omega_0 \ll \Omega_{\rm i}$. In the case of the Crab pulsar, $t = 918$ yr and this is in remarkably good agreement with the age estimated from historical astronomical observations of 1243 yr (Shapiro & Teukolsky, 1984). Also, assuming the Crab pulsar to be a NS with typical mass $M = 1.4 M_\odot$ and radius $R = 12$ km, eq. (4) allows to determine a MF $B_{\rm p} = 5.2 \times 10^{12}$ G.

In practice, observations provide $\Omega(t)$ and its time derivatives. Assuming a generic power-law dependence for the rate of change in the spin $\dot{\Omega} = d\Omega/dt = -(\text{const.})\Omega^n < 0$, we can measure the *"braking index"* n as

$$n = -\frac{\Omega\ddot{\Omega}}{\dot{\Omega}^2} \,. \tag{6}$$

Using eq. (5), we readily obtain $n = 3$, which is to be compared with the observed value of $n \simeq 2.515$ and where a number of factors can be invoked to explain the differences.

2.2 The Magnetosphere

Although the rotating dipole model discussed above provides explanations for many of the observed properties of pulsars, it is based on the hypothesis that the rotator is in vacuum. As shown by Goldreich & Julian (1969), this is rather unrealistic and the EF induced by the rotation of the magnetic moment is sufficient to pull-out charges from the stellar surface. These will then corotate with the star, forming the so-called *"magnetosphere"*.

Many models have followed the original aligned rotator model by Goldreich & Julian (1969). However, because the latter contains the most important features which have then been shared also by more complex (and realistic) models I will briefly describe it. Consider therefore a perfectly conducting rotating sphere threaded by an external dipolar MF given by

$$\mathbf{B}_{(\rm ext)} = B_{\rm p} R^3 \left(\frac{\cos\theta}{r^3}\,\mathbf{e}_r + \frac{\sin\theta}{2r^3}\,\mathbf{e}_\theta \right) \ . \tag{7}$$

Because of the perfect conductivity (i.e. $\sigma \to \infty$) in the stellar interior, Ohm's law will be

$$\frac{\mathbf{j}_{(\rm int)}}{\sigma} = 0 = \mathbf{E}_{(\rm int)} + \frac{\mathbf{\Omega}\times\mathbf{r}}{c} \times \mathbf{B}_{(\rm int)} \ , \tag{8}$$

so that the interior EMFs are mutually orthogonal [i.e. $(\mathbf{E}\cdot\mathbf{B})_{(\rm int)} = 0$]. Assuming now that no surface currents are present, the continuity across the stellar surface of the normal and tangential components of the MF indicate that the form of the interior EMFs is

$$\mathbf{B}_{(\rm int)} = B_{\rm p} \left(\cos\theta\,\mathbf{e}_r + \frac{\sin\theta}{2}\,\mathbf{e}_\theta \right) \ , \tag{9}$$

$$\mathbf{E}_{(\rm int)} = \frac{\Omega R B_{\rm p} \sin\theta}{c} \left(\frac{\sin\theta}{2}\,\mathbf{e}_r - \cos\theta\,\mathbf{e}_\theta \right) \ . \tag{10}$$

Similarly, by requiring the continuity of the tangential EF we obtain

$$E^\theta_{(\rm ext)} = E^\theta_{(\rm ext)} = -\frac{\Omega R B_{\rm p} \sin\theta}{c} \frac{\partial}{\partial\theta} \left(\frac{\sin^2\theta}{2} \right) \ . \tag{11}$$

Stated differently, the rotation of the magnetic dipole moment induces an quadrupolar EF.

Note that the EM in the exterior could well not be orthogonal and, in particular

$$(\mathbf{E}\cdot\mathbf{B})_{(\rm ext)} = -\frac{\Omega R}{c} B_{\rm p}^2 \left(\frac{R}{r}\right)^7 \cos^3\theta \ , \tag{12}$$

so that the external EF component parallel to the MF will be

$$\left(\frac{\mathbf{E}\cdot\mathbf{B}}{|\mathbf{B}|}\right)_{(\rm ext)} \sim \frac{\Omega R}{c} B_{\rm p} \sim 2 \times 10^8 \left(\frac{1\ {\rm sec}}{P}\right)\left(\frac{B_{\rm p}}{10^{12}\ {\rm G}}\right) \ . \tag{13}$$

The electric force acting on charged particles at the stellar surface is $\sim e\mathbf{E}_{\rm ext}$ and is far larger than the corresponding gravitational one

$$\left(\frac{\text{electric force}}{\text{gravitational force}}\right) \sim \frac{e\Omega R B_{\rm p}/c}{GMm_e/R^2} \sim 10^9 \ . \tag{14}$$

As a result, charged particles will be extracted from the stellar surface and will fill the magnetosphere which corotates rigidly with the star.

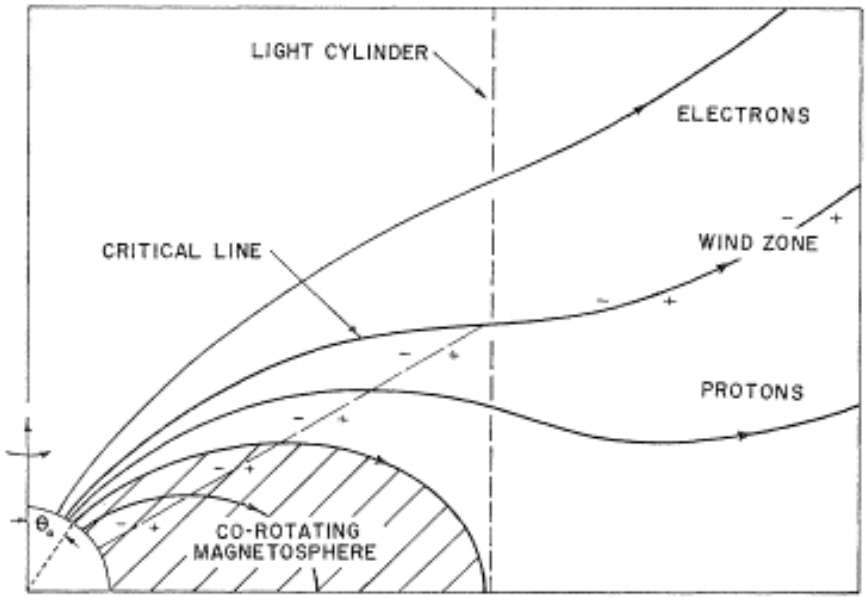

Figure 1: Schematic representation of the magnetosphere and MF lines in the aligned rotator model (from Goldreich & Julian 1969).

In the magnetosphere the EM are orthogonal ($\mathbf{E}\cdot\mathbf{B}=0$) and the charge distribution is

$$\rho_{\rm e}=\frac{1}{4\pi}\nabla\cdot\mathbf{E}=\frac{1}{2\pi c}\mathbf{\Omega}\cdot\mathbf{B}\,. \tag{15}$$

Because of corotation, the MF lines of the magnetosphere will be closed out to *"light cylinder"* $r_c\equiv c/\Omega$. The MF lines that cross r_c are open and deflected back to form a toroidal MF. Charged particles are accelerated along these lines ($\mathbf{E}\cdot\mathbf{B}\neq 0$) and stream out to infinity, producing the pulsed emission observed.

As a final comment, it is useful to underline that the estimates on the strength of the MF coming from the lines in the spectra of X-ray pulsars and from the spin-down measurements are in general agreement. However, new evidence is now mounting that the two observations may be sensitive to two distinct MFs (either at the surface or at large distances from it) and that the two MFs can also be considerably different.

It is now important to discuss how the intense MF can be produced and for this a minimal approach to the equations of magnetohydrodynamics is necessary and will be done in the following Section.

3 Introduction to the MHD Equations

Consider a globally neutral plasma of particles of charge $\pm e$ (e.g. electrons and protons) at the same temperature T_0 and with mean particle density n_0. The charge densities will be

$$n_{\rm e}(\phi) = n_0 e^{e\phi/T_0} \simeq n_0(1 + \frac{e\phi}{T_0}), \qquad\qquad n_{\rm p}(\phi) = n_0 e^{-e\phi/T_0} \simeq n_0(1 - \frac{e\phi}{T_0}), \tag{16}$$

where ϕ is the electrostatic potential and we have assumed that $|e\phi/|T_0 \ll 1$, i.e. the kinetic energy is larger than the inter-particle potential. In such a "weakly coupled" plasma, a test charge $q_{\rm t}$ at the origin will experience the global electrostatic potential solution of the Poisson equation

$$\nabla^2\phi = 4\pi e[n_{\rm e}(\phi) - n_{\rm p}(\phi)] - 4\pi q_{\rm t}\delta^{(3)}(\mathbf{x}), \tag{17}$$

or, using eqs. (16) and (17),

$$\nabla^2\phi - \frac{1}{\lambda_{\rm D}^2}\phi = -4\pi q_{\rm t}\delta^{(3)}(\vec{x}), \tag{18}$$

where

$$\lambda_{\rm D} = \sqrt{\frac{T_0}{8\pi n_0 e^2}}, \tag{19}$$

is the *Debye length*. Stated differently, the global effect of the presence other particles in the plasma will be such that the test particle will experience a Coulomb potential that is screened at large distances by a Yukawa term, i.e. $e^{-r/\lambda_{\rm D}}$, i.e. like in a mutual exclusion.

Since the particles in the plasma exchange momentum through two-body interactions with a cross-section $\sigma \sim \alpha_{\rm em}^2/T_0^2$, where $\alpha_{\rm em}$ is the electromagnetic coupling constant, the mean-free-path will be $\ell_{\rm mfp} \sim T_0^2/(\alpha_{\rm em}^2 n_0)$ and thus [cf. eq. (19] $\lambda_{\rm D} \ll \ell_{\rm mfp}$. In other words, $\ell_{\rm mfp}$ is not the smallest lengthscale in the plasma which is a weakly collisional system not

in local thermodynamical equilibrium in general.

Recalling now that the thermal velocity of an electron of mass $m_{\rm e}$ is $v_{\rm ther} \simeq \sqrt{T_0/m_{\rm e}}$, the collision frequency will be $\omega_{\rm c} \simeq v_{\rm ther}/\ell_{\rm mfp}$. This is much smaller than the plasma frequency, i.e. the oscillation frequency of the electrons when displaced from their equilibrium in a background of approximately fixed ions

$$\omega_{\rm p} = \sqrt{\frac{4\pi n_0 e^2}{m_{\rm e}}} \gg \omega_{\rm c}, \tag{20}$$

so that the system undergoes many oscillations between two collisions.

A measure of the state of plasma is obtained with the *plasma parameter* $\mathcal{N} \equiv 1/(n_0 \lambda_{\rm D}^3)$, basically counting the number of particles in the Debye sphere or, equivalently, the number of particles interacting. Since $\mathcal{N} \propto n_0^{-1}$, the number of particles interacting in a low-density

plasma is larger and basically because the Debye shielding is less effective. Note also that

$$\frac{\text{potential energy of interactions}}{\text{kinetic energy}} \sim \frac{e^2 n_0^{1/3}}{T_0} = \mathcal{N}^{2/3}. \tag{21}$$

Hence, in a low-density plasma $\mathcal{N}$ is small and the interactions are weak and the opposite is true for a high-density plasma. Note that almost 99% of the baryonic matter in the Universe is in a plasma state.

The weakly coupled plasma with $\mathcal{N} \ll 1$ has a complete mathematical description in terms of kinetic theory, but this is often exceedingly complicated. However, alternative and simpler approaches are possible. In particular, in a weakly collisional plasma the typical lengthscale L and a timescale τ are such that

$$L \gg \lambda_{\rm D}, \qquad\qquad \tau \gg \omega_{\rm p}^{-1}\,. \tag{22}$$

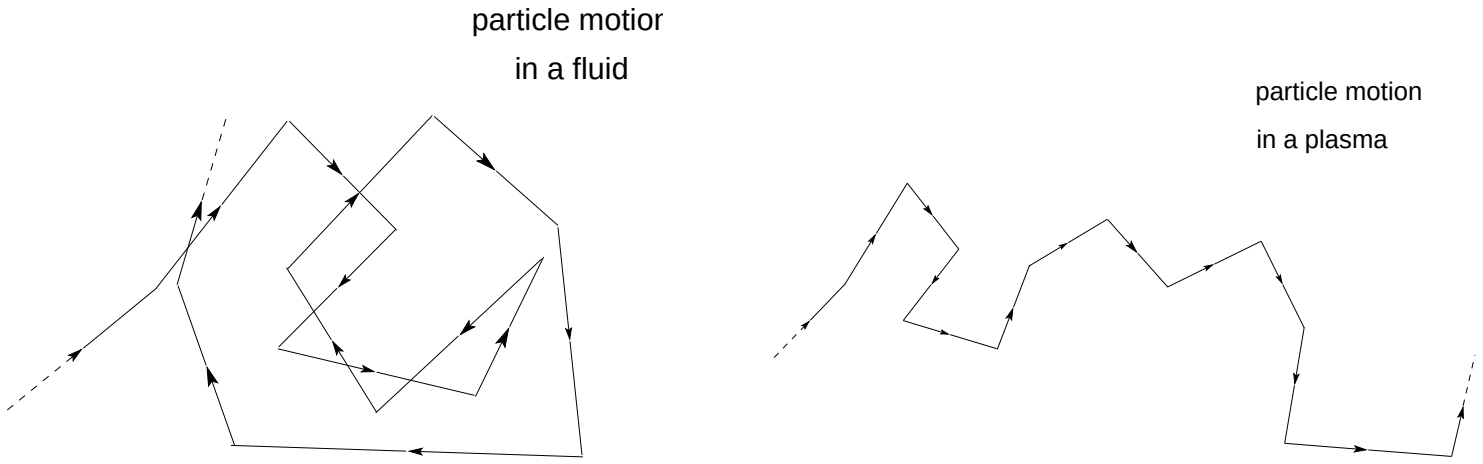

Figure 2: Schematic difference of the particle motion in a fluid and in a plasma, where global EMFs determine the secular motion.

In the case of a plasma, therefore, charged particles will not be influenced by the EMFs of the other particles up until they enter in their Debye sphere. However, long-range EMFs are present and determine the collective motions (see Fig. 2 for a schematic example).

One can then adopt a fluid description derived directly from kinetic theory in a *mean-field* approach in which the hydrodynamics equations are "corrected" because of the global EMFs threading the plasma. In this approach, the dynamics of the plasma as a fluid is

described by the magnetohydrodynamic (MHD) equations

$$\frac{\partial \rho}{\partial t} + \nabla \cdot (\rho \mathbf{v}) = 0, \qquad \text{(continuity equation)} \tag{23}$$

$$\frac{\partial \rho_{\mathrm{e}}}{\partial t} + \nabla \cdot \mathbf{j} = 0, \qquad \text{(charge conservation equation)} \tag{24}$$

$$\frac{\partial \mathbf{v}}{\partial t} + (\mathbf{v} \cdot \nabla)\, \mathbf{v} = -\nabla \Phi - \frac{1}{\rho} \nabla p + \frac{1}{\rho} \mathbf{j} \times \mathbf{B}, \qquad \text{(Euler equations)} \tag{25}$$

$$\mathbf{j} = \sigma \left(\mathbf{E} + \mathbf{v} \times \mathbf{B} \right) - \frac{\sigma}{e n_0} (\mathbf{j} \times \mathbf{B} - \nabla p_e). \qquad \text{(Ohm's law)} \tag{26}$$

where Φ is the gravitational potential, $\mathbf{j} \equiv e n_0 \mathbf{v}$ the charge-density current, σ the electric conductivity and p_{e} the electron pressure, and the term $\mathbf{j} \times \mathbf{B}$ represents the Lorentz force.

Besides an equation of state (EOS) relating pressure and mass density, the set of eqs. (23)–(26) is completed by the Maxwell equations

$$\nabla \cdot \mathbf{E} = 4\pi\rho_{\rm e}, \qquad \nabla \cdot \mathbf{B} = 0, \tag{27}$$

$$\frac{\partial \mathbf{B}}{\partial t} + \nabla \times \mathbf{E} = 0, \qquad \frac{\partial \mathbf{E}}{\partial t} = \nabla \times \mathbf{B} - 4\pi\mathbf{j}. \tag{28}$$

On lengthscales much larger than $\lambda_{\rm D}$, the plasma is effectively neutral and the charge density in (24) and (27) can be neglected to yield EFs and currents that are solenoidal

$$\nabla \cdot \mathbf{j} = 0, \qquad \nabla \cdot \mathbf{E} = 0. \tag{29}$$

Similarly, on timescales much longer than the ones of the plasma oscillations, the displacement current in eqs (28) can be neglected to yield

$$\nabla \times \mathbf{B} = 4\pi\mathbf{j}. \tag{30}$$

Using now (30) in the Euler equations (25) and simple vector manipulations we obtain

$$\frac{\partial \mathbf{v}}{\partial t} + (\mathbf{v}\cdot\nabla)\,\mathbf{v} \;=\; -\nabla\Phi - \frac{1}{\rho}\nabla p + \frac{1}{4\pi\rho}(\nabla\times\mathbf{B})\times\mathbf{B}$$

$$\;=\; -\nabla\Phi - \frac{1}{\rho}\nabla\left(p + p_{\rm mag}\right) + \frac{1}{4\pi\rho}(\mathbf{B}\cdot\nabla)\mathbf{B}, \qquad (31)$$

where $p_{\rm mag} \equiv B^2/(8\pi)$ is the *"magnetic pressure"* orthogonal to the MF lines, while the term $(\mathbf{B}\cdot\nabla)\mathbf{B}$ represents a *"magnetic tension"* along the MF lines.

Given the Euler equation (31), it is possible to define a *force-free* MF as the one for which $(\nabla\times\mathbf{B})\times\mathbf{B} = 0$ and this approximation is often used in astrophysical flows.

3.1 The Induction Equation and the Alfvén Theorem

One of the most important MHD is clearly the *induction equation* (28) expressing the time evolution of the MF. A useful expression for it can be obtained after noting that the the Hall (i.e. $\propto \mathbf{j} \times \mathbf{B}$) and thermoelectric (i.e. $\propto \nabla p_{\rm e}$) terms in the right-hand-side of Ohm's law are usually very small in the MHD approach, so that effectively

$$\mathbf{j} \simeq \sigma \left(\mathbf{E} + \mathbf{v} \times \mathbf{B} \right) . \tag{32}$$

Using (32) and (30) we can write the induction equation as

$$\frac{\partial \mathbf{B}}{\partial t} = \nabla \times \left(\mathbf{v} \times \mathbf{B} \right) - \nabla \times \left(\eta \, \nabla \times \mathbf{B} \right) , \tag{33}$$

where $\eta \equiv 1/(4\pi\sigma)$ is the *magnetic diffusivity*. Even in the case of adiabatic flows (i.e. neglecting all energetic losses due to MF reconnection of electromagnetic radiation), eqs. (33) and (31) are responsible for the complexity of the dynamics of magnetized plasmas. Par-

ticularly interesting and relevant for the remainder are two limits of (33).

The first one is referred to as the *"ideal MHD"* limit and is the one corresponding to an infinite conductivity i.e. $\eta \to 0$, for which (33) reduces to

$$\frac{\partial \mathbf{B}}{\partial t} = \nabla \times (\mathbf{v} \times \mathbf{B}) \,. \tag{34}$$

It is now not difficult to show that the Lagrangian time derivative $d/dt = \partial/\partial t + v^i \partial/\partial x^i$ of the integral of the MF over any surface made of fluid elements will be zero, i.e.

$$\frac{d}{dt} \int_S \mathbf{B} \cdot d\,\mathbf{S} = 0. \tag{35}$$

Since the Lagrangian time derivative implies that we are considering the variation in time while comoving with the fluid elements, eq. (35) basically states that in highly conducting plasma the MF is advected with the fluid and is "frozen-in" when $\sigma \to \infty$. This is known as Alfvén theorem and is the equivalent of Kelvin's theorem for vorticity.

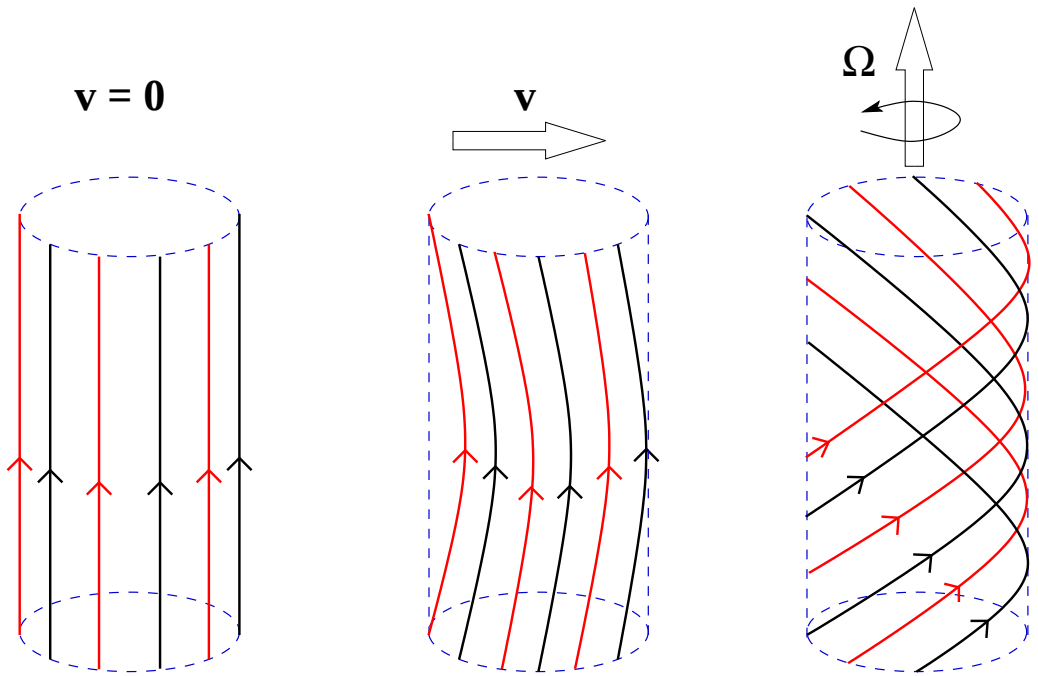

Figure 3: Schematic illustration of the magnetic flux freezing. The sequence shows a MF flux tube which is static (left), is sheared by a transversal velocity field (middle) and is twisted by rotation.

Another quantity conserved in the ideal-MHD limit is the magnetic helicity defined as

$$\mathcal{H}_M = \int_V (\mathbf{A} \cdot \mathbf{B}) d^3x \ , \qquad \text{with} \qquad \mathbf{B} = \nabla \times \mathbf{A}, \tag{36}$$

where $\mathbf{A}$ is the vector potential. The conservation of helicity expresses the fact that the MF does not change topology via magnetic reconnection.

The other important limit of eq. (33) is the *"resistive-MHD"* limit and it appears for zero fluid motions (i.e. $\mathbf{v} = 0$), so that (33) reduces to the parabolic equation

$$\frac{\partial \mathbf{B}}{\partial t} = -\nabla \times (\eta \, \nabla \times \mathbf{B}) = \eta \, \nabla^2 \mathbf{B} \, , \tag{37}$$

where the last expression is valid when the diffusivity does not depend on space. Being a parabolic equation, expression (37) simply states that a MF with scale L will *decay* on a timescale $\tau_{\rm diff} = 4\pi L^2 \sigma$ and that $\mathbf{B}(t) \rightarrow 0$ for $t \rightarrow \infty$. Estimating the electrical conductivity of NS matter to be (Lamb 1991)[1]

$$\sigma \approx 10^{26} \left(\frac{10^8 \ {\rm K}}{T} \right)^2 \left(\frac{\rho}{10^{14} \ {\rm g \ cm^{-3}}} \right)^{3/4} \ {\rm s^{-1}} \, , \tag{38}$$

the MF of a NS varying on a scale $L \simeq 0.1R$ will have a magnetic diffusion timescale

$$\tau_{\rm diff} = 4\pi L^2 \sigma \approx 3 \times 10^6 \left(\frac{\Delta R}{10^5 \ {\rm cm}} \right)^2 \left(\frac{10^9 \ {\rm K}}{T} \right)^2 \left(\frac{\rho}{10^{14} \ {\rm g \ cm^{-3}}} \right)^{3/4} \ {\rm yr} \, . \tag{39}$$

[1]Note that expression (38) is roughly correct for densities in the range $10^{10} - 10^{14}$ g cm^{-3} and temperatures in the range $10^6 - 10^8$ K, but provides a reasonable estimate also at temperatures of $\sim 10^9 - 10^{10}$ K which are the relevant ones for the r-mode instability (Potekhin et al. 1999).

4 Generation of Magnetic Fields in PNSs and NSs

The origin of the strong MFs in NSs is still a matter of controversy. The MFs inferred from the pulsar spin-down data ranges from $\sim 5 \times 10^{13}$ to $\sim 10^{8}$ G but these values are representative of the global dipolar magnetic configuration rather than of the fine magnetic structure near the stellar surface. X-ray spectra of some pulsars and the cyclotron lines they contain, provide a closer look at the MF strength near the NS surface and suggest a surface MF, $B_s \sim 1.5 \times 10^{14}$ G (Sanwal et al. 2002). This is to be contrasted with the dipolar MF estimated from the spin-down rate: $B_d \sim (2-4) \times 10^{12}$ G (Pavlov et al. 2002).

For many years the MFs in NSs have been simply related to the MFs of the progenitor main-sequence stars frozen during collapse and amplified by flux conservation [cf. Alfvén theorem (35)]: an initial surface MF of ~ 100 G and a reduction in radius of a factor $\sim 10^{5}$

are in fact sufficient to reach a MF amplification of 10^{10}.

This view, however, is now challenged by the difficulty of having sufficiently strong seed fields in the progenitors and by the evidence that the local MFs at the NS surface can be well above the dipolar one responsible for the spin-down.

On the other hand, MFs with different strengths on different length-scales can be explained naturally if they are generated through a dynamo mechanism driven by turbulent motions. It is generally accepted that PNSs are subject, shortly after their birth, to hydrodynamic instabilities involving convective motions (Epstein 1979, Livio et al. 1980, Burrows & Lattimer 1986) and that these can last $\sim 30 - 40$ s (Miralles et al. 2000, 2002).

I will show that, under suitable conditions, turbulent motions can generate MF via dynamo action (Bonanno et al. 2003) and that a mean-field dynamo can be operative together with a small-scale dynamo (Thompson & Duncan 1993; Xu & Busse 2001).

4.1 Convection in PNSs

Hydrodynamic instabilities in PNSs can be driven by either lepton gradients (Epstein 1979) leading to the so-called *"neutron-finger instability"* (Bruenn & Dineva 1996), or by negative entropy gradients which are commonly observed in simulations of supernova explosions (Bruenn & Mezzacappa 1994, 1995; Rampp & Janka 2000) and evolutionary models of PNSs (Keil & Janka 1995; Keil et al. 1996; Pons et al. 1999). This latter instability is usually referred to as the *"convective instability"*.

Despite their names, note that *both* instabilities involve convective motions, ie motions of large cells that rise, expand, "thermalize" and fall back.

The evolution of these instabilities can be summarized as follows:

- the instabilities will first develop in the outer layers containing $\sim 30\%$ of the stellar mass, with the convectively unstable region surrounded by the neutron-finger unstable region, the latter involving therefore a larger portion of the stellar material.
- After a few seconds the two unstable regions move towards the inner parts of the star and after ~ 10 s from the initial development, more than 90% in mass of the star is hydrodynamically unstable. The stellar core has become convectively unstable but it is still surrounded by an extended neutron-finger unstable region.
- In the ~ 20 s that follow, the temperature and lepton gradients are progressively reduced and the two unstable regions begin to shrink, leaving the outer regions of the star.
- After ~ 30 s, most of the PNS is stable and the instabilities disappear after ~ 40 s (Miralles et al. 2000).

Note: because the PNS is opaque to neutrinos, the turbulent mean velocity can be estimated within the mixing-length approximation.

Using the pressure length-scale, $L \equiv p|dp/dr|^{-1}$, the effective flow velocity in this scale can be estimated as $v_{_L} \approx L/\tau_{_L}$, where $\tau_{_L}$ is the growth-time of instability which is of the order of the turnover time in the scale L.

In the *convectively unstable* region, the growth-time of instability is

$$\frac{1}{\tau_{_L}^2} \sim \frac{1}{\tau_c^2} \sim \frac{1}{3} g\beta \frac{|\Delta\nabla T|}{T} \,, \tag{40}$$

where τ_c is the growth-time of convection, g is the gravitational acceleration, $\Delta\nabla T$ is the difference between the actual and the adiabatic temperature gradient, and β is the coefficient of thermal expansion. Except during the last stages of the unstable phase, the convective instability grows on a short dynamical timescale. Miralles et al. (2000), have estimated this to be $\tau_c \sim 0.1 - 1$ ms, so that $v_{_L} \sim 10^8 - 10^9$ cm s^{-1}.

In the *neutron-finger unstable* region, on the other hand, the lepton number gradients dominate over the temperature gradients and we can estimate the growth-time as

$$\frac{1}{\tau_L^2} \sim \frac{1}{\tau_{nf}^2} \sim \frac{1}{3} g \delta |\nabla Y| \,, \tag{41}$$

where δ is the coefficient of chemical expansion, and $Y = (n_e + n_\nu)/n$ is the lepton fraction with n_e, n_ν, and n being the number density of electrons, neutrinos, and baryons, respectively. The estimated growth-time in the neutron-finger unstable region is a couple of orders of magnitude *longer* than the one for the convective instability, i.e. $\tau_{nf} \sim 30 - 100$ ms (Miralles et al. 2000), thus yielding a mean turbulent velocity $v_{_L} \sim (1-3) \times 10^6$ cm s^{-1}.

In 1993 Thompson & Duncan proposed that a small-scale dynamo can operate in the turbulent stages of the PNS's life. The MFs produced in this way were close to equipartition $B \sim 10^{15}$ G and were used to propose the idea of *magnetars* to account for the phenomenol-

ogy observed in soft γ-ray repeaters (Duncan & Thompson 1992).

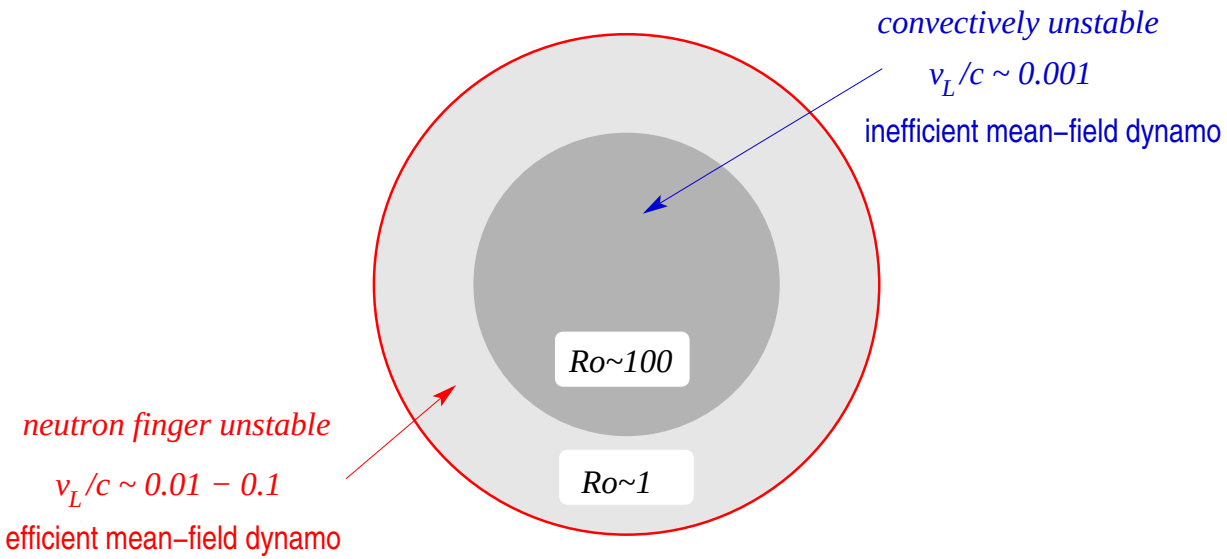

Figure 4: Schematic representation of the two convective zone in a a PNS. Note the two mean turbulent velocities resulting from the two growth timescales in the two unstable regions and the different Rossby numbers Ro in the two regions.

Note that in the model by Thompson & Duncan (1993) the whole PNS to be convectively unstable with turbulent velocity $v_L \sim 10^8$ cm s^{-1}.

The existence of two unstable regions with substantially different mean velocities is a

significant difference because the efficiency of the mean-field dynamo will be different in the two regions and particularly high in the neutron-finger unstable region.

PNSs, in fact, are likely to rotate and although the initial spin rates of pulsars are not well constrained by observations, they are believed to be $P \sim 100$ ms (Narayan 1987). As a result, the Rossby number Ro will be

$$R_o \equiv \frac{P}{\tau_L} \sim \begin{cases} 1 & \text{convectively unstable region ,} \\ 100 & \text{neutron finger region ,} \end{cases} \tag{42}$$

As a consequence, in the convectively unstable region the influence of rotation on the turbulence is weak and the mean-field dynamo will be inefficient here. In the neutron-finger unstable region, on the other hand, turbulence can be strongly modified by rotation and a mean-field dynamo is more efficient. In both regions turbulent MFs can also be generated by small-scale dynamo driven by turbulent motions.

4.2 Dynamo Action in PNSs

Because the characteristic cooling timescale for the PNS exceeds both τ_{nf} and τ_c, the turbulence can be treated adiabatically (this assumption will cease to be accurate as the instabilities are progressively suppressed). In this case, the mean-field induction equation for a turbulent, magnetised and conducting plasma can be written as

$$\frac{\partial \mathbf{B}}{\partial t} = \nabla \times (\mathbf{v} \times \mathbf{B} + \alpha \mathbf{B}) - \nabla \times (\widetilde{\eta}\, \nabla \times \mathbf{B}) \,, \tag{43}$$

where $\widetilde{\eta}$ is the turbulent magnetic diffusivity, α is a pseudo-scalar measuring the efficiency of the "alpha-dynamo". Here, $\mathbf{v}$ is the velocity the ordered fluid motion, which we assume to follow a simple law, $\mathbf{v} = \mathbf{\Omega} \times \mathbf{r}$, but allow for the differential rotation $\mathbf{\Omega} = \mathbf{\Omega}(r)$, where $\Omega(r) = \Omega_0 + r^2\Omega_1$. Because the coupling between the induction and Euler equations is neglected, the MF evolution will grow following a *kinetic dynamo* process.

But *what is a dynamo action?*

Loosely speaking, a velocity field $\mathbf{v}$ is responsible for a dynamo when its interaction with the MF is such that the latter does not decay in time asymptotically.

More rigorously, a continuous velocity field $\mathbf{v}$ is responsible for a dynamo when there exists an initial MF configuration and a finite magnetic diffusivity such that the evolution of the MF via the induction equation (33) leads to a non-zero value of the total magnetic energy

$$E_{\rm M} \equiv \frac{1}{8\pi} \int_{V_\infty} \mathbf{B}^2 d^3\mathbf{x} \,, \tag{44}$$

as $t \to \infty$ (Moffatt 1978). The asymptotic total magnetic energy can either tend to a constant (non-zero) value, oscillate about such value or increase without limit: i.e $E_{\rm M} \not\to 0$ as $t \to \infty$. Note that a velocity field is either capable of a dynamo action or not.

In a rotating turbulence with lengthscale ℓ and moderate Rossby number, the α-parameter can be estimated to be $\alpha \approx -\Omega\ell^2\nabla\ln(\rho v_L^2)$ (Rüdiger & Kitchatinov 1993) but because in PNSs the density scale-height is comparable to the pressure one L, we express the isotropic turbulence in the neutron-finger unstable zone simply as $\alpha_{nf} \approx \Omega L$.

Given a certain amount of differential rotation, the seed MF will grow if $\alpha_{nf} > \alpha_0$ and instead decay if $\alpha_{nf} < \alpha_0$. The different types of dynamo can be distinguished according to whether the differential rotation is small and the evolution of the MF stationary (i.e. a α^2-dynamo), or the differential rotation is large and the MF oscillating (i.e. a $\alpha\Omega$-dynamo).

Since $\alpha_{nf} \approx \Omega L$, the critical value α_0 effectively selects a critical value for the spin period, $P_0 \equiv 2\pi L/\alpha_0$, such that *MF generation via a mean-field dynamo action will possible if the stellar spin period is shorter than the critical one.*

The induction equation (43) with given profiles η and α which have a sharp transition at the core-radius R_c has been solved numerically in axisymmetry by Bonanno, Rezzolla and Urpin (2003) varying progressively the degree of differential rotation $q \equiv R^2\Omega_1/\Omega(r=R)$ to determine the critical value α_0 corresponding to the marginal stability of the dynamo. A couple of comments are worth making

- $q<0$ and $q>0$ correspond to situations in which the stellar surface rotates faster and slower than the centre, respectively (values $q<-1$ correspond to a counter-rotation and may be not physically relevant).
- A stationary α^2-dynamo dominates the MF generation process for $|q|<1$, while a $\alpha\Omega$-dynamo is more efficient for $|q|>1$. In this case, the MF will be of oscillating strength but, given the large differential rotation required, it may be difficult to achieve.

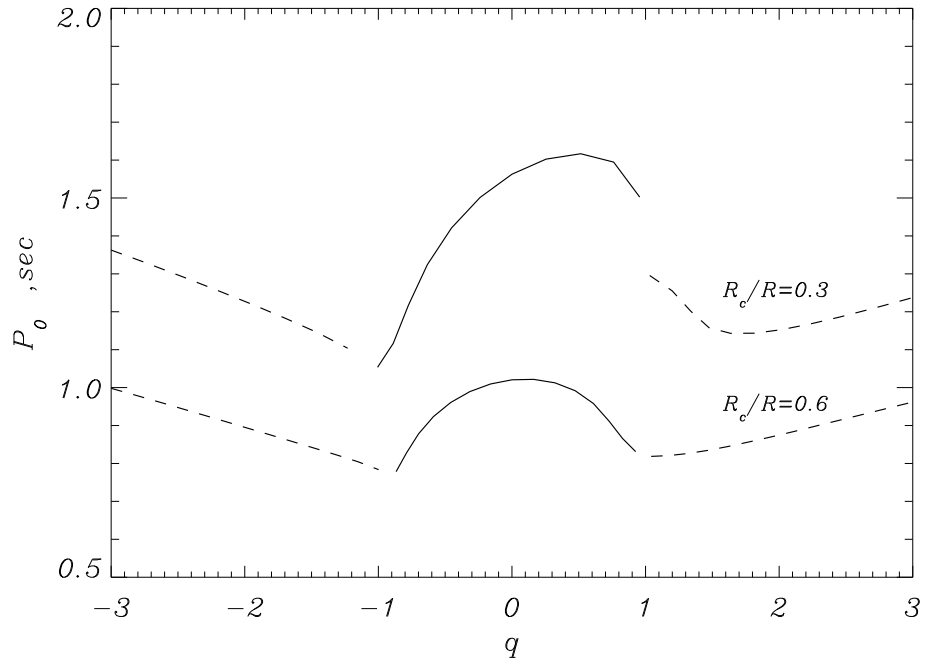

Figure 5: Critical period as a function of the differential rotation parameter. The two curves refer to different values of R_c, with the solid parts corresponding to a α^2-dynamo and the dashed parts to a $\alpha\Omega$-dynamo.

In Fig. 5, I show the critical period as a function of the differential rotation parameter q. The two curves refer to different values of R_c, with the solid parts corresponding to a α^2-dynamo and the dashed parts to a $\alpha\Omega$-dynamo.

The results of the calculations can be summarized as follows

- for a PNS rotating uniformly (i.e. $q = 0$), a mean-field dynamo will develop if $P \leq 1$ s when $R_c/R = 0.6$ and if $P \leq 1.5$ s when $R_c/R = 0.3$.
- for a PNS rotating differentially with $|q| \approx 1$, P_0 is further reduced of $\sim 20\%$.
- the α^2-dynamo is the most likely source of MF generation in PNSs.
- the final value of the MF cannot be estimated but the efficiency of the dynamo could produced yield values close to equipartition (i.e. $B \sim 10^{15}$ G) as suggested in *magnetars*.

As a result, *only PNSs with* $P \gtrsim 1 - 1.5$ *s will not develop* a turbulent mean-field dynamo. Such slow rotation rates should be rather difficult to achieve if angular momentum is conserved during the collapse to a PNS. These result indicate therefore that a turbulent mean-field dynamo could be effective during the initial stages of the life of most PNSs.

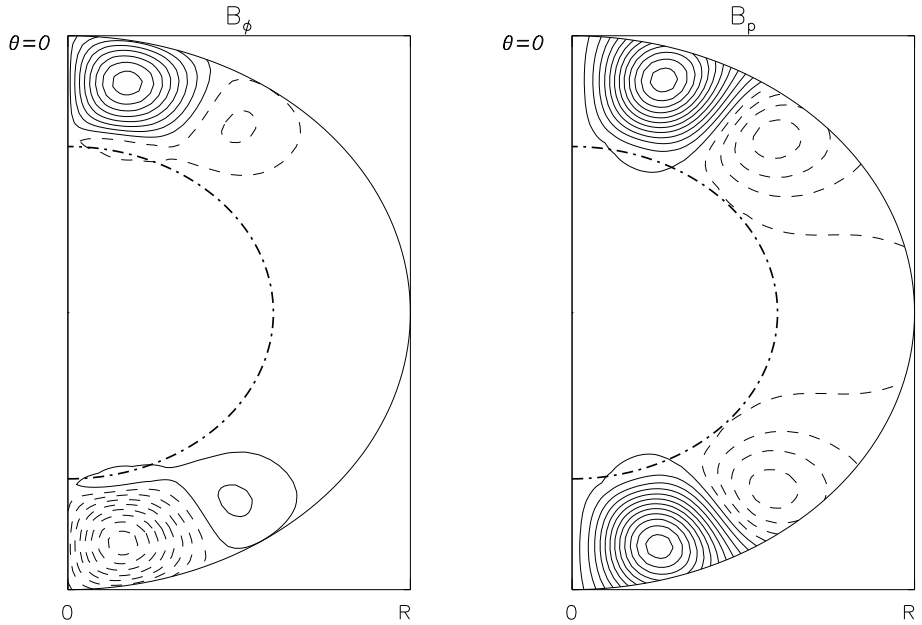

Figure 6: Toroidal (B_ϕ) and poloidal (B_p) MF lines. Solid and dashed contours correspond to positive and negative values, respectively. The dot-dashed line marks the position of $R_c = 0.6R$.

In Fig. 6 I show the toroidal (B_ϕ) and poloidal (B_p) MFs of a typical PNS model. Note that both components are generated in the outer neutron-finger unstable region, but turbulent diffusion produces a much weaker MF also in the inner convectively unstable region.

The toroidal MF tends to concentrate near the polar regions whereas the poloidal one is more evenly distributed in latitude. The numerical calculations also show that

- if $|q| < 1$ and the field is generated by the α^2-dynamo, then $B_\phi/B_p \sim 10$;
- if $|q| > 1$ and the field is generated by the $\alpha\Omega$-dynamo, then $B_\phi/B_p \sim 100 - 200$.

Both results suggest that the internal MFs in NSs could be substantially stronger than the observable surface ones.

5 Magnetic Fields produced by Stellar Instabilities

Hydrodynamic instabilities inevitably involve a series of processes which are often coupled and in nonlinear manners. The picture does not improve when MFs are present which provide in general a new channel for in which the energy in the system can flow, either adiabatically or not. It will not surprise, therefore, that general statements on the role of MFs in generic instabilities are difficult if not impossible to make.

However, when the instability is the amplification of stellar oscillations through the generic CFS mechanism (Chandrasekhar 1970, Friedman & Schutz 1978), it is clear that the evolution of the oscillations in magnetized NSs will be affected not only by gravitational radiation and viscous dissipation, but also by the loss of rotational and mode energy to electromagnetic radiation and the growth of the stellar MF.

The generation of MF, in particular, is a generic feature of shearing flows perpendicular to MF lines in a highly conducting plasma, such as hot NS matter. This reflects the fact that, in such conditions, the MF is predominantly advected with the fluid [cf. Alfvén theorem (35)].

5.1 The case of the r-mode Instability

Since r-mode oscillations produce large scale mass-currents, it is natural to expect that these could couple with the MF present in the NS, offering a new sink for the energy of the mode. Note that a linear r-mode oscillation would produce a shearing flow distorting the MF, this distortion would be *periodic*, averaging to zero after each oscillation. As a result, an effectively shearing flow will be present only if *secular* motions are superimposed to the periodic ones and are produced by nonlinear effects.

In a series of papers (Rezzolla et al. 2000, 2001a, 2001b) it was pointed out that nonlinear kinematic effects can be deduced (at least qualitatively) already from the linear equations of motion. These effects give rise to a secular velocity field which, once coupled to any seed MF, will produce exponentially growing MFs as the instability develops.

If the MF produced as a result of this coupling is strong enough, it can distort significantly the r-mode oscillations so as prevent the amplification of r modes by gravitational radiation. If, on the other hand, the MF is initially weak, it will be subsequently amplified and cause the instability to die out as the star spins down.

In what follows I will first briefly show how to deduce the nonlinear secular velocity field and then discuss the properties of the MF produced.

5.1.1 Linear and Nonlinear Kinematics

Consider the motion of fiducial fluid elements on an isobaric surface of a rotating star experiencing r-mode oscillations. In an orthonormal basis, and at first order in the star's unperturbed angular velocity Ω, such perturbations may be written as

$$\delta\mathbf{v}(r,\theta,\phi,t) = \alpha\Omega R\left(\frac{r}{R}\right)^{\ell}\mathbf{Y}^{B}_{\ell m}e^{i\sigma t}\ , \tag{45}$$

where R is the radius of the unperturbed star, α is the dimensionless amplitude of the perturbation and σ is the frequency of the mode in the inertial frame, related to the frequency in the corotating frame as

$$\sigma = \omega - \ell\Omega = -\frac{(\ell-1)(\ell+2)}{\ell+1}\Omega\ . \tag{46}$$

In a frame instantaneously corotating with the star the equations of motion of fiducial fluid elements of an $\ell = m$ mode are

$$\dot{r}(t,\theta,\phi) = 0 \ , \tag{47}$$

$$\dot{\theta}(t,\theta,\phi) = \alpha\Omega \left(\frac{r}{R}\right)^{\ell-1} c_\ell \sin\theta (\sin\theta)^{\ell-2} \cos\left[\ell\phi + \left(\frac{2\Omega}{\ell+1}\right) t\right] \ , \tag{48}$$

$$\dot{\phi}(t,\theta,\phi) = -\alpha\Omega \left(\frac{r}{R}\right)^{\ell-1} c_\ell \cos\theta (\sin\theta)^{\ell-2} \sin\left[\ell\phi + \left(\frac{2\Omega}{\ell+1}\right) t\right] \ , \tag{49}$$

where c_ℓ is a constant coefficient. Clearly, eqs. (47)–(49) produce perfectly periodic oscillations and no MF over a period.

When the nonlinear expressions are not available it is possible to calculate second-order quantities from linear results (Landau & Lifschitz 1987, Lighthill 1980). This is an approximation but in some relevant examples, such as sound waves and shallow water waves, the secular *nonlinear* drift velocity is given exactly to $\mathcal{O}(\alpha^2)$ by the *linear* velocity field.

In particular, we have expanded the equations of motion in powers of α, averaged over a gyration, and retained only the lowest-order non-vanishing term. In this way we find that $\mathcal{O}(\alpha^2)$ drift velocity exists in the $\phi-$direction and is given by

$$\mathbf{v}_{\rm d}(r,\theta,t) = \frac{2}{3}\kappa_2(\theta)\alpha^2(t)\Omega(t)R\left(\frac{r}{R}\right)^2 \mathbf{e}_{\hat{\phi}}\,, \tag{50}$$

where $\kappa_2(\theta) \equiv (1/2)^7(5!/\pi)(\sin^2\theta - 2\cos^2\theta)$ (Rezzolla et al. 2000) and $\mathbf{e}_{\hat{\phi}}$ the unit vector in the ϕ-direction. It is important to underline that the secular velocity field (50) is responsible for a differential rotation in both the radial and polar directions and that the latter has been qualitatively confirmed both in simplified models (Levin & Ushomirsky 2000) and in fully nonlinear simulations (Stergioulas & Font 2000, Lindblom et al. 2000).

It is important to emphasise that using the equations of motion (47)–(49) to compute the displacement of an element of fluid expanding $\dot{\theta}$ and $\dot{\phi}$ in powers of α is not equivalent

to considering nonlinear effects in the fluid equations but provides a first approximate answer (which is indeed exact in the case of shallow water waves). More recently, a systematic investigation at second-order in α has shown that the expression (50) does indeed provide a very good approximation to the exact $\mathcal{O}(\alpha^2)$ expression (Sá 2003).

Using (50), the total displacement in ϕ from the onset of the oscillation at t_0 up to time t is then found to be (At second-order in α there is no secular motion in the $\theta-$direction.)

$$\Delta\tilde{x}^{\phi}(r,t) \equiv \int_{t_0}^{t} \delta v^{\phi}(t')dt' = \frac{2}{\ell+1}\left(\frac{r}{R}\right)^{\ell-1}\kappa_{\ell}(\theta)\int_{t_0}^{t}\alpha^2(t')\Omega(t')dt' + \mathcal{O}(\alpha^3)\ . \tag{51}$$

with $t \gg \Omega^{-1}$. Note that even if $\Omega = \text{const.}$, a net secular azimuthal motion is obtained *both* when the mode's amplitude is constant [i.e. $\mathcal{O}(\alpha^2 t)$] and when the mode's amplitude is exponentially growing in time [i.e. $\mathcal{O}(\alpha_0^2 \exp(2t/\tau_{\text{GW}}))$, where α_0 is the initial mode amplitude and τ_{GW} is the timescale for the instability to develop].

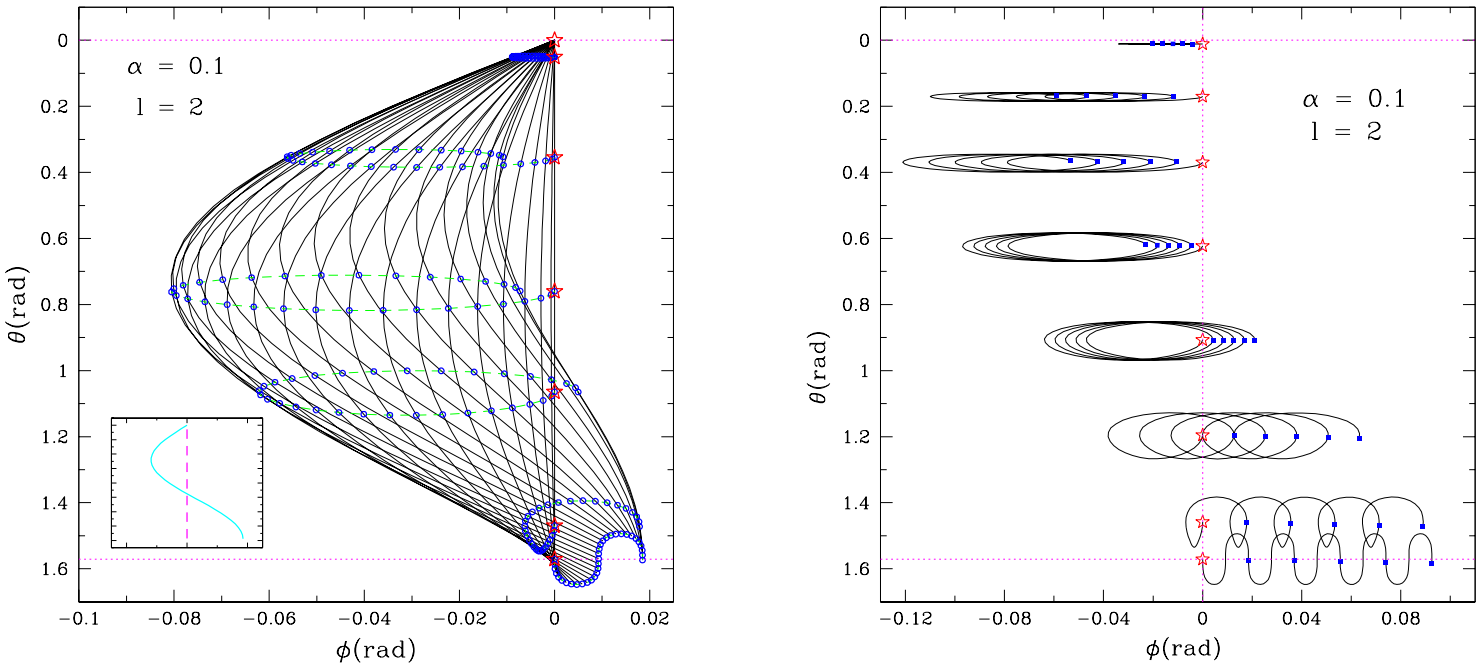

Figure 7: Projected trajectories of seven fiducial fluid elements as seen in the corotating frame over *one period* (left diagram) or over *five periods* (right diagram) for a r-mode oscillation with $\ell = 2$, $\alpha = 0.1$. The inset shows the initial (continuous) and final (dashed) positions.

In Fig. 7 I show numerical integrations of the equations of motion (48) and (49) on the northern hemisphere of the rotating star and the inset in the left panel shows schematically the initial (dashed) and final positions of the fluid elements after one cycle (continuous).

Several interesting properties can be deduced from Fig. 7:

a) the trajectories over one period $\omega/2\pi$ are *not* closed;

b) while the excursions in the θ and ϕ directions are comparable, the net displacement $\Delta\phi$ in longitude after one cycle is much larger than the net displacement $\Delta\theta$ in latitude.

c) both $\Delta\phi$ and $\Delta\theta$ are linearly proportional to α;

d) the motions have a simple dependence on latitude.

All of the relevant information about the secular behaviour is contained in (51) and (50) and these expressions can be used to study the interaction between r-mode oscillations and any MF present in the rotating NS.

5.2 Evolution of the Magnetic Field: a Lagrangian approach

I start with combining the equation of mass conservation

$$\frac{d\rho}{dt} = -\rho \left(\nabla \cdot \mathbf{v} \right) \ , \tag{52}$$

where $d/dt \equiv (\partial/\partial t + \mathbf{v} \cdot \nabla)$, with the induction equation in the ideal MHD limit

$$\frac{\partial \mathbf{B}}{\partial t} = \nabla \times \left(\mathbf{v} \times \mathbf{B} \right) \ , \tag{53}$$

to obtain

$$\frac{D}{Dt} \left(\frac{\mathbf{B}}{\rho} \right) = \left(\frac{\mathbf{B}}{\rho} \cdot \nabla \right) \delta \mathbf{v} \ , \tag{54}$$

where $\mathbf{v} = \mathbf{\Omega} \times \mathbf{r} + \delta \mathbf{v}$ and $D/Dt \equiv (\partial/\partial t + \mathbf{v} \cdot \nabla - \mathbf{\Omega} \times)$ is the Lagrangian derivative for a fluid element moving at velocity $\mathbf{v}$ as seen in the corotating frame.

Eq. (54) can be integrated analytically to give (Parker 1979)

$$\frac{B^j}{\rho}(\tilde{\mathbf{x}},t) = \frac{B^k}{\rho}(\mathbf{x},t_0)\frac{\partial \tilde{x}^j(t)}{\partial x^k(t_0)} \ . \tag{55}$$

Note that $\nabla \cdot \mathbf{\Omega} \times \mathbf{r} = 0$ at first order in the stellar angular velocity and $\nabla \cdot \delta\mathbf{v} = 0$ by definition of axial perturbations. As a result, to lowest order in Ω and α the flow is therefore incompressible and we can set $\rho(\tilde{\mathbf{x}},t) = \rho(\mathbf{x},t_0)$. The integral form (55) of the induction equation is particularly advantageous as it shows that the MF at time t and position $\tilde{\mathbf{x}}$ can be computed from the MF at time t_0 and position $\mathbf{x}$, using the tensorial coordinate strain $\partial\tilde{x}^j(t)/\partial x^k(t_0)$ that develops between t_0 and t. The advection of MF lines is an obvious consequence of Eq. (55) and the problem of the MF evolution is therefore transformed into the problem of determining the time evolution of the strain tensor $S_{jk} \equiv \partial\tilde{x}^j/\partial x^k$.

5.3 An Analytical model of the r-mode instability

While full numerical calculations are possible to compute the evolution of the instability and the solution of the induction eq. (55), I will here present a simplified but analytic picture of the instability and calculate the generation of very large toroidal MFs as a result of the azimuthal secular velocity field produced by the instability.

The expressions for the time evolution of the angular velocity and mode amplitude during the period of activity of the instability (Owen et al. 1998) can be approximated as

$$\Omega(t) \simeq \begin{cases} \Omega_0 & \text{if } t \leq t_{\rm sat} \ , \\ \Omega_0 \left[1 + C_1 \Omega_0^{2\ell+2} (t - t_{\rm sat})\right]^{-(2\ell+2)} & \text{if } t > t_{\rm sat} \ , \end{cases} \tag{56}$$

$$\alpha(t) \simeq \begin{cases} \alpha_0 \, \exp(t/|\tau_{\rm GW}|) & \text{if } t \leq t_{\rm sat} \ , \\ \alpha_{\rm sat} & \text{if } t > t_{\rm sat} \ . \end{cases} \tag{57}$$

with C_1 a constant coefficient (Rezzolla et al. 2001). Using (56) and (57), Eq. (51) can be integrated to give

$$\tilde{x}^{\phi}(t) = \begin{cases} \left(\frac{r}{R}\right) \frac{\kappa_2 \Omega_0 \alpha_0^2}{2} |\tau_{\rm GW}| \left[\exp(2t/|\tau_{\rm GW}|) - 1\right] , & \text{if } t \leq t_{\rm sat} , \\ \left(\frac{r}{R}\right) \frac{\kappa_2 \Omega_0 \alpha_0^2}{2} |\tau_{\rm GW}| \left[\exp(2t/|\tau_{\rm GW}|) - 1\right] + \\ \qquad \left(\frac{6r}{5R}\right) \frac{(\kappa_2)^2 \alpha_{\rm sat}^2}{C_1 \Omega_0^5} \left\{ \left[1 + C_1 \Omega_0^6 (t - t_{\rm sat})\right]^{5/6} - 1 \right\} , & \text{if } t > t_{\rm sat} . \end{cases} \tag{58}$$

As a result, the average MF produced at a given time as a result of the shearing secular drift (58) of a predominantly poloidal MF (i.e. $B^{\phi}(\mathbf{x}, t_0) \ll B^{r}(\mathbf{x}, t_0) \sim B^{\theta}(\mathbf{x}, t_0)$)

$$B^{\phi}(\tilde{\mathbf{x}}, t) = B^{r}(\mathbf{x}, t_0) \frac{\tilde{x}^{\phi}(t)}{r} + B^{\theta}(\mathbf{x}, t_0) \frac{\partial \tilde{x}^{\phi}(t)}{\partial \theta} . \tag{59}$$

For a *"fiducial" NS* spinning at the mass-shedding limit and for which the instability is free to develop, on a timescale $|\tau_{\rm GW}| \simeq 37$ s for the $\ell = m = 2$ mode, the mode will saturate at $\alpha_{\rm sat} = 0.1$ after $t_{\rm sat} \simeq 430$ s. In this case, the volume averaged toroidal magnetic fields at saturation and after one year can be estimated to be respectively

$$\langle \Delta B^{\hat{\phi}}(t = t_{\rm sat}) \rangle \simeq \int_{\rm V_*} \left[B_0^{\hat{r}} + \frac{2}{\pi} B_0^{\hat{\theta}} \right] \tilde{x}^{\hat{\phi}} \, d^3\mathbf{x} \sim 3.9 \times 10^2 \, \langle B_0^{\hat{p}} \rangle \, {\rm G} \, , \tag{60}$$

$$\langle \Delta B^{\hat{\phi}}(t = 1{\rm yr}) \rangle \sim 1.2 \times 10^8 \, \langle B_0^{\hat{p}} \rangle \, {\rm G} \, . \tag{61}$$

Stated differently, in the absence of a back-reaction on the dynamics of the r-mode instability, the toroidal MF is tightly wrapped around the star so as to become about two orders of magnitude larger that the seed poloidal MF by the time the instability reaches saturation and eight orders of magnitude larger on a timescale of one year.

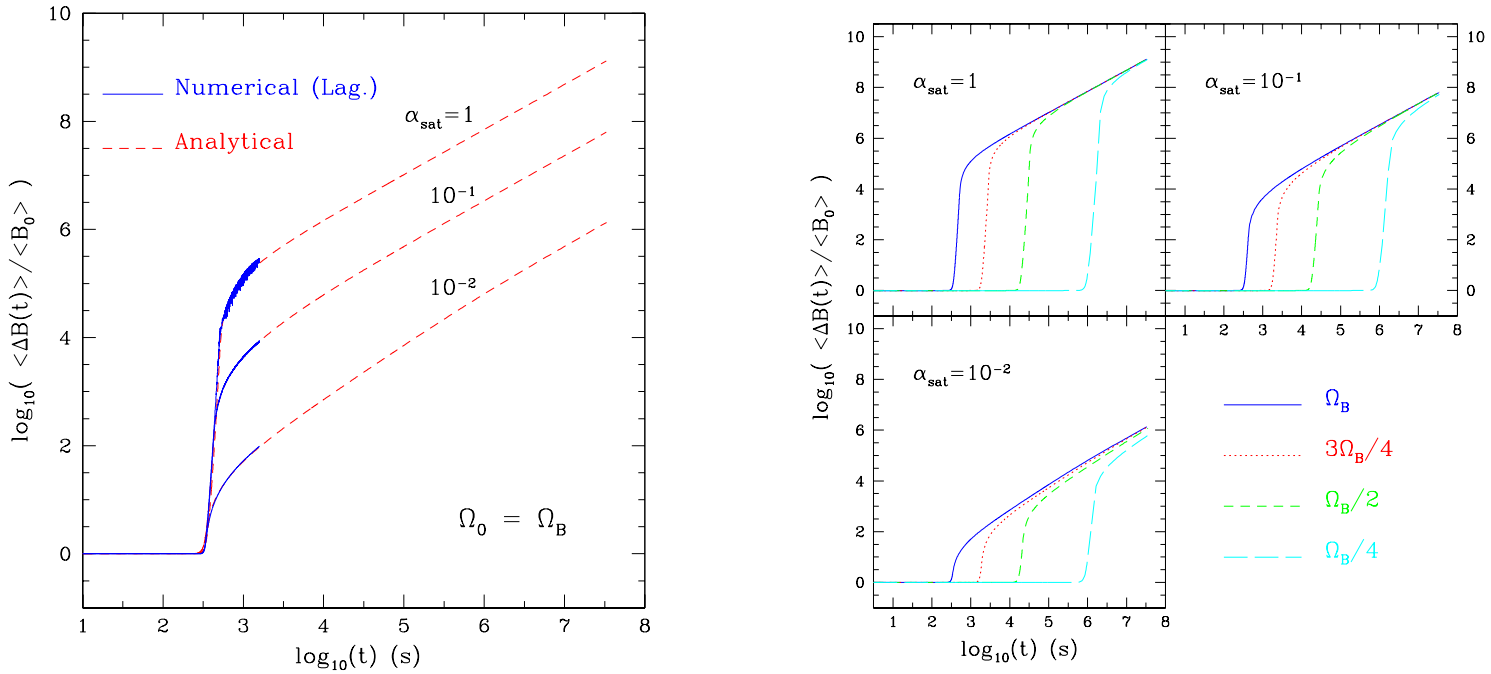

Figure 8: Left panel: evolution of the total secular magnetic field $\langle \Delta B \rangle$ scaled to the initial field for an $\ell = 2$ mode and different saturation amplitudes. Right panel: changes in the evolution resulting from different values of the initial angular velocity.

The simple estimates outlined above already show that an initial MF $B_0^{\hat{p}}$ could produce, after one year, an equipartition toroidal MF of $\sim 10^{15}$ G, i.e. a toroidal MF whose energy is comparable with the rotational energy of the star.

TO SUMMARISE:

- r modes distort the MFs of NSs and their occurrence can be limited by this interaction;
- a velocity drift is produced which leads to differential rotation and loss of vorticity
- if the MF is $\gtrsim 10^{16}\,(\Omega/\Omega_B)$ G with Ω_B the break-up spin, r modes cannot occur;
- much weaker MFs will prevent gravitational radiation from exciting r-mode oscillations or damp them on a relatively short timescale by extracting energy from the modes faster than GW emission can pump energy into them.
- E.g.: a 10^{10} G poloidal MF threading the star's superconducting core can prevent the $\ell = 2$ mode from being excited unless $\Omega \gtrsim 0.35\Omega_B$;
- E.g.: if $\Omega \gtrsim 0.35\Omega_B$ initially, the $\ell = 2$ mode may be excited but will decay once Ω falls below $0.35\Omega_B$; this happens in $\lesssim 15$ days if $\alpha_{\rm sat} \gtrsim 0.1$.

LAST BUT NOT LEAST:

An important issue remains unresolved and is whether the magnetic field will distort the r-mode velocity field in such a fine-tuned way so as to cancel the fluid drift before it suppresses the oscillation.

Assessing this requires a modelling beyond a kinematic dynamo, but is worth pointing out that the fractional change in the mode energy produced by GW emission during a single oscillation period is $4\pi/\omega|\tau_{GW}|$ and is always smaller than the change in magnetic energy for typical MF strengths in NS.

6 Structure and Stability of Highly Magnetized Relativistic NSs

Using a pseudo-spectral method, Bocquet et al. (1995) have calculated the first numerical solutions of the coupled Einstein-Maxwell equations for stationary, rotating and magnetized NSs.

In the solutions found the equilibrium is the result of the balance among the gravitational force, the pressure gradients and the Lorentz force produced by an electric current whose distribution in the star can be freely specified.

The MF field considered was axisymmetric and poloidal (a toroidal MF would break the "circularity"[2] of the spacetime) in vacuum[3], the rotation uniform (the only compatible with stationarity) and different EOSs.

[2] A spacetime is "circular"if a coordinate system (t, r, θ, ϕ) can be found such that the components of the metric tensor are zero except for the diagonal terms and only one off-diagonal term ($g_{t\phi}$). In the non-circular case, only one component can be set to zero ($g_{r\theta}$).

[3] Here vacuum refers to the a region with zero baryon number. In this region, however, EMFs are present and provide a nonzero stress-energy tensor.

The most important results of these investigations can be summarized as follows:

- highly magnetized star will have an additional magnetic pressure so that the star will support larger maximum masses at the same central density and rotation rate;
- in the case of nonrotating stars, the maximum mass can be $M \simeq 1.9 - 4M_{\odot}$ depending on the EOS; the maximum MF at the stellar centre and pole are $B \simeq 9.0 - 30.2 \times 10^{17}$ G;
- for a configuration with a dipolar MF the Lorentz forces on the conducting fluid behave as centrifugal forces producing a "flattening" of the stellar surface;
- the deformation induced by the EM stresses for a fixed magnetic moment depends on the MF distribution and hence on details of the electric current distribution in the star;
- a stochastic MF or a superconducting stellar interior greatly increases the efficiency of the magnetic dipole to distort the star, leading to detectable GW radiation;

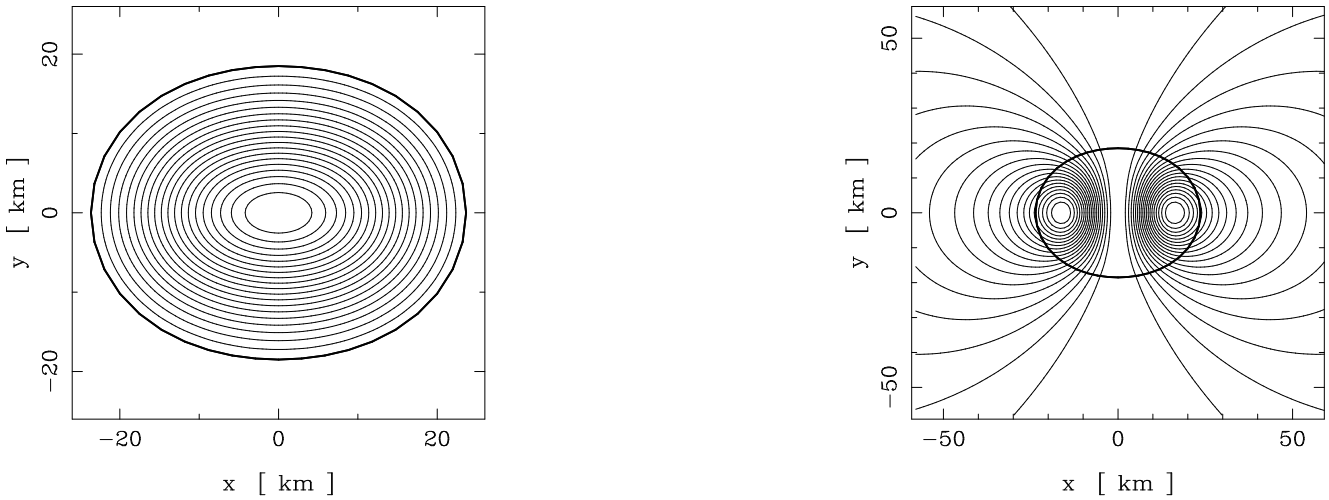

Figure 9: Left panel: isocontours of the rest-mass density of a static magnetized star of $2.98\,M_\odot$ built on the Pol2 EOS of Salgado et al. (1994a). Right panel: MF lines for the same model; the MF strength is $B = 3.57 \times 10^{17}$ G at the star's centre and $B = 9.1 \times 10^{16}$ G at the north pole (Figs from Bocquet et al. 1995).

Even in the static case, the stress-energy tensor of the EMF is not isotropic and that the star deviates from spherical symmetry. For large MFs this deviation becomes apparent as shown in Fig. 9. Note the flattened shape produced by the Lorentz forces and reminescent of the oblateness produced by centrifugal forces.

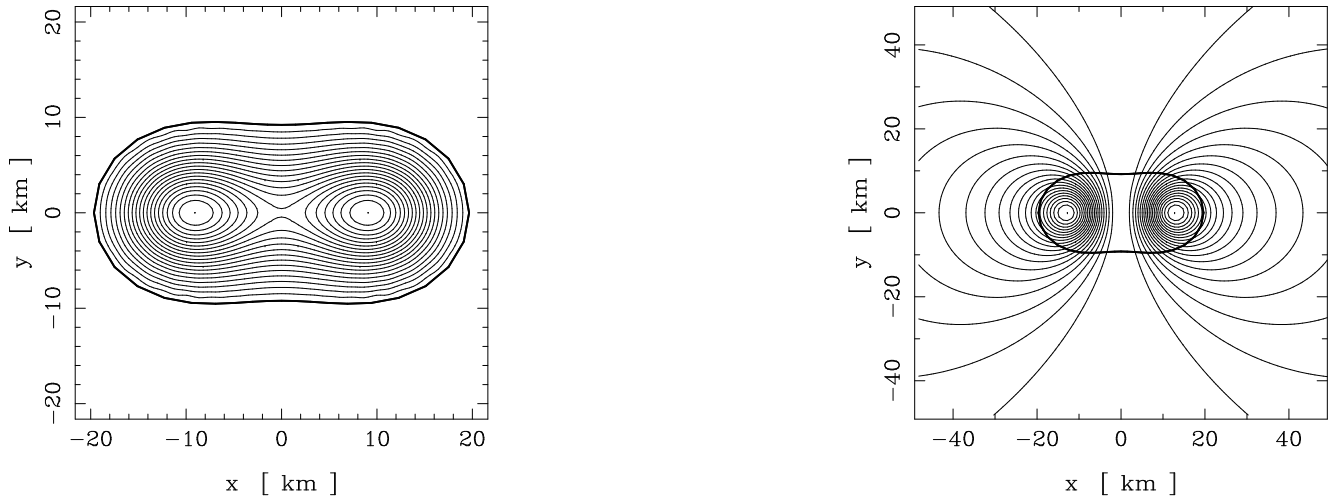

Figure 10: The same as in Fig. 9 but for a rotating magnetized star of $4.06\,M_{\odot}$, the maximum possible. The MF strength is $B = 9.0 \times 10^{17}$ G at the star's centre and $B = 4.6 \times 10^{16}$ G at the north pole (Figs. from Bocquet et al. 1995).

Fig. 10 is the same as Fig. 9 but for a rotating star and in particular for the one with the maximum mass. Note that the rest-mass density maximum is not at the centre of the star.

When the value of the central MF is high enough for the magnetic pressure $p_{\rm mag}$ to be equal the fluid pressure p, the total stress tensor S_{ij} has a vanishing component along the symmetry axis. Away from the centre and along the axis, p decreases more rapidly than $p_{\rm mag}$ so that a "pinch" is produced along the symmetry axis.

7 General Relativistic Electrodynamics of NSs

The investigation of the general relativistic corrections to the solution of Maxwell equations in the spacetime of a relativistic star has a long history. The initial works of Ginzburg & Ozernoy (1964), Anderson & Cohen (1970) and of Petterson (1974) on the stationary electromagnetic fields (EMFs) in a Schwarzschild spacetime have revealed that the spacetime curvature produces MFs which are generally stronger than their Newtonian counterparts (Wasserman & Shapiro 1983) and that the decay time is smaller but comparable with the one found in flat spacetime (Geppert et al. 2000)

The effects induced by the rotation of the star are less known and were first investigated by Muslimov & Tsygan (1992) in the slow rotation approximation. A similar approach was used by Muslimov and Harding (1997) for the EMFs external to a rotating magnetized star.

More recently, a systematic investigation has been carried out by Rezzolla et al. (2001, 2002, 2003, 2004) to derive in a form as analytic as possible the expressions for test EMFs of spherical and rotating relativistic stars. In what follows I will only briefly report the essential results, remanding to the above papers for the numerous and lengthy expressions.

Let us start by considering the background of a stationary, axially symmetric rotating star truncated at the first order in the angular velocity Ω (Hartle & Thorne 1968)

$$ds^2 = -e^{2\Phi(r)}dt^2 + e^{2\Lambda(r)}dr^2 - 2\omega(r)r^2\sin^2\theta dt d\phi + r^2 d\theta^2 + r^2\sin^2\theta d\phi^2 \,, \tag{62}$$

where $\omega(r)$ is the Lense-Thirring angular velocity and is the solution of an ODE in the stellar interior, while outside the star it is expressed as

$$\omega(r) \equiv \frac{d\phi}{dt} = -\frac{g_{0\phi}}{g_{\phi\phi}} = \frac{2J}{r^3} \tag{63}$$

Here, J and I are total angular momentum and momentum of inertia, respectively.

The general form of the first pair of general relativistic Maxwell equations is given by

$$3!F_{[\alpha\beta,\gamma]} = 2\left(F_{\alpha\beta,\gamma} + F_{\gamma\alpha,\beta} + F_{\beta\gamma,\alpha}\right) = 0\ . \tag{64}$$

where $F_{\alpha\beta}$ is the electromagnetic tensor. For an observer with four-velocity u^{α}, the covariant components of the electromagnetic tensor are given by (Misner et al. 1974)

$$F_{\alpha\beta} \equiv 2u_{[\alpha}E_{\beta]} + \eta_{\alpha\beta\gamma\delta}u^{\gamma}B^{\delta} = u_{\alpha}E_{\beta} - u_{\beta}E_{\alpha} + \eta_{\alpha\beta\gamma\delta}u^{\gamma}B^{\delta}\ . \tag{65}$$

where $\eta_{\alpha\beta\gamma\delta}$ is the Levi-Civita pseudo-tensor. The second pair of Maxwell equations is

$$F^{\alpha\beta}{}_{;\beta} = 4\pi J^{\alpha} \tag{66}$$

where the four-current J^{α} is a sum of convection and conduction currents such that

$$J^{\alpha} = \rho_{\mathrm{e}}w^{\alpha} + j^{\alpha}\ , \qquad j_{\alpha} = \sigma F_{\alpha\beta}w^{\beta}\ , \qquad j^{\alpha}w_{\alpha} \equiv 0\ , \tag{67}$$

with $\boldsymbol{w}$ being the conductor four-velocity.

A particularly useful class of observers is represented by the *"zero angular momentum observers"* or *ZAMOs* (Bardeen et al. 1972). These are observers that are locally stationary (i.e. at fixed values of r and θ) but who are "dragged" into rotation with respect to a reference frame fixed with respect to distant observers. At first order in Ω they have four-velocity components given by ZAMOs carry a tetrad with components

$$\boldsymbol{e}^{\alpha}_{\hat{0}} = e^{-\Phi}\Big(1,0,0,\omega\Big)\ , \quad \boldsymbol{e}^{\alpha}_{\hat{r}} = e^{-\Lambda}\Big(0,1,0,0\Big)\ , \tag{68}$$

$$\boldsymbol{e}^{\alpha}_{\hat{\theta}} = \frac{1}{r}\Big(0,0,1,0\Big)\ , \quad \boldsymbol{e}^{\alpha}_{\hat{\phi}} = \frac{1}{r\sin\theta}\Big(0,0,0,1\Big)\ . \tag{69}$$

and such that in this tetrad the EM tensor has the same components as in a flat spacetime. Once expressed in this tetrad, the Maxwell equations have a much simpler form, in which the general relativistic corrections are more easily distinguished from the Newtonian parts

$$\sin\theta\left(r^2B^{\hat{r}}\right)_{,r}+e^{\Lambda}r\left(\sin\theta B^{\hat{\theta}}\right)_{,\theta}+e^{\Lambda}rB^{\hat{\phi}}{}_{,\phi}=0\,, \tag{70}$$

$$(r\sin\theta)\frac{\partial B^{\hat{r}}}{\partial t}=e^{\Phi}\left[E^{\hat{\theta}}{}_{,\phi}-\left(\sin\theta E^{\hat{\phi}}\right)_{,\theta}\right]-(\omega r\sin\theta)\,B^{\hat{r}}{}_{,\phi}\,, \tag{71}$$

$$\left(e^{\Lambda}r\sin\theta\right)\frac{\partial B^{\hat{\theta}}}{\partial t}=-e^{\Phi+\Lambda}E^{\hat{r}}{}_{,\phi}+\sin\theta\left(re^{\Phi}E^{\hat{\phi}}\right)_{,r}-\left(\omega e^{\Lambda}r\sin\theta\right)B^{\hat{\theta}}{}_{,\phi}\,, \tag{72}$$

$$\left(e^{\Lambda}r\right)\frac{\partial B^{\hat{\phi}}}{\partial t}=-\left(re^{\Phi}E^{\hat{\theta}}\right)_{,r}+e^{\Phi+\Lambda}E^{\hat{r}}{}_{,\theta}+\sin\theta\left(\omega r^2B^{\hat{r}}\right)_{,r}+\omega e^{\Lambda}r\left(\sin\theta B^{\hat{\theta}}\right)_{,\theta}\,, \tag{73}$$

and

$$\sin\theta\left(r^2E^{\hat{r}}\right)_{,r}+e^{\Lambda}r\left(\sin\theta E^{\hat{\theta}}\right)_{,\theta}+e^{\Lambda}rE^{\hat{\phi}}{}_{,\phi}=4\pi e^{\Lambda}r^2\sin\theta J^{\hat{t}}\,, \tag{74}$$

$$e^{\Phi}\left[\left(\sin\theta B^{\hat{\phi}}\right)_{,\theta}-B^{\hat{\theta}}{}_{,\phi}\right]-(\omega r\sin\theta)\,E^{\hat{r}}{}_{,\phi}=r\sin\theta\frac{\partial E^{\hat{r}}}{\partial t}+4\pi e^{\Phi}r\sin\theta J^{\hat{r}}\,, \tag{75}$$

$$e^{\Phi+\Lambda}B^{\hat{r}}{}_{,\phi}-\sin\theta\left(r\,e^{\Phi}B^{\hat{\phi}}\right)_{,r}-\left(\omega e^{\Lambda}r\sin\theta\right)E^{\hat{\theta}}{}_{,\phi}=e^{\Lambda}r\sin\theta\frac{\partial E^{\hat{\theta}}}{\partial t}+4\pi e^{\Phi+\Lambda}r\sin\theta J^{\hat{\theta}}\,, \tag{76}$$

$$\left(e^{\Phi}rB^{\hat{\theta}}\right)_{,r}-e^{\Phi+\Lambda}B^{\hat{r}}{}_{,\theta}+\sin\theta\left(\omega r^2E^{\hat{r}}\right)_{,r}+\omega e^{\Lambda}r\left(\sin\theta E^{\hat{\theta}}\right)_{,\theta}=e^{\Lambda}r\frac{\partial E^{\hat{\phi}}}{\partial t}+4\pi e^{\Lambda}r(e^{\Phi}J^{\hat{\phi}}+\omega r\sin\theta J^{\hat{t}})\,. \tag{77}$$

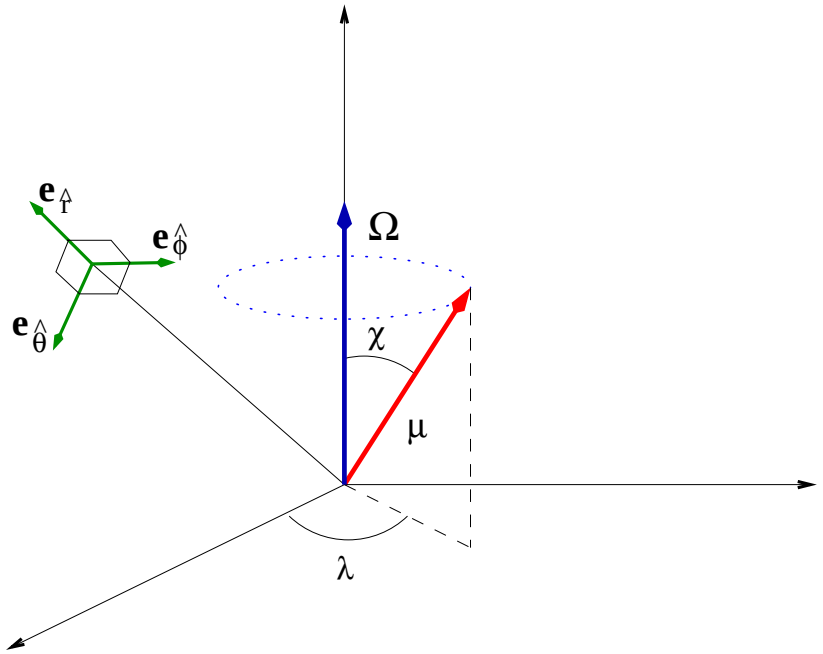

Figure 11: Schematic representation of a misaligned rotator. Here $(\boldsymbol{e}_{\hat{0}}, \boldsymbol{e}_{\hat{r}}, \boldsymbol{e}_{\hat{\theta}}, \boldsymbol{e}_{\hat{\phi}})$ is a local orthonormal frame, $\boldsymbol{\mu}$ is the magnetic dipole moment of the star, χ is the inclination angle relative to the rotation axis, and λ the instantaneous azimuthal position.

The problem is easy to formulate. Consider a perfectly conducting magnetic dipole μ rotating in vacuum: *what are the EMFs observed at a large distance but within the light cylinder (i.e. near-zone)?* The solution to this problem dates back to the work of Deutsch (1959) and is a landmark result in the electrodynamics of pulsars.

Skipping the details on the derivation, the solution for the MF components is

$$B^{\hat{r}} = \frac{2\mu}{r^3}\left(\cos\chi\cos\theta + \sin\chi\sin\theta\cos\lambda\right) \ , \tag{78}$$

$$B^{\hat{\theta}} = \frac{\mu}{r^3}\left(\cos\chi\sin\theta - \sin\chi\cos\theta\cos\lambda\right) \ , \tag{79}$$

$$B^{\hat{\phi}} = \frac{\mu}{r^3}\sin\chi\sin\lambda \ , \tag{80}$$

while the corresponding EFs are given by

$$E^{\hat{r}} = -\frac{\mu\Omega R^2}{cr^4}\left[\cos\chi(3\cos^2\theta - 1) + 3\sin\chi\cos\lambda\sin\theta\cos\theta\right] \ , \tag{81}$$

$$E^{\hat{\theta}} = -\frac{\mu\Omega}{cr^2}\left\{\frac{2R^2}{r^2}\cos\chi\sin\theta\cos\theta + \sin\chi\left[1 - \frac{R^2}{r^2}(\cos^2\theta - \sin^2\theta)\right]\cos\lambda\right\} \ , \tag{82}$$

$$E^{\hat{\phi}} = \frac{\mu\Omega}{cr^2}\sin\chi\cos\theta\sin\lambda\left(1 - \frac{R^2}{r^2}\right) \ . \tag{83}$$

Three interesting features of solutions (78)–(80) and (81)–(83) should be noticed.

- the periodic time modulation introduced by the precession of the magnetic moment, disappearing when the dipole is aligned, i.e. for $\chi = 0$

- the toroidal components of the EMFs are just a by-product of the misalignment between the rotation axis and the magnetic dipole and again disappear when $\chi = 0$.

- an EF of $\mathcal{O}(\Omega)$ introduced by the rotation of the sphere and whose quadrupolar part [i.e. $\propto (3\cos^2\theta - 1)/2$] is present also when $\chi = 0$; this is the rotation-induced EF.

7.2 Rotating Magnetized Conductor in a Slowly Rotating Spacetime: Exterior Solution in the Near-Zone

I now consider the equivalent problem in General Relativity and for a slowly rotating spacetime. Skipping again the details, the solution for the MF is (Rezzolla et al. 2001)

$$B^{\hat{r}} = -\frac{3}{4M^3}\left[\ln N^2 + \frac{2M}{r}\left(1+\frac{M}{r}\right)\right](\cos\chi\cos\theta + \sin\chi\sin\theta\cos\lambda)\mu\ , \tag{84}$$

$$B^{\hat{\theta}} = \frac{3N}{4M^2 r}\left[\frac{r}{M}\ln N^2 + \frac{1}{N^2} + 1\right](\cos\chi\sin\theta - \sin\chi\cos\theta\cos\lambda)\mu\ , \tag{85}$$

$$B^{\hat{\phi}} = \frac{3N}{4M^2 r}\left[\frac{r}{M}\ln N^2 + \frac{1}{N^2} + 1\right](\sin\chi\sin\lambda)\mu\ , \tag{86}$$

while for the EFs this is given by (Rezzolla et al. 2001)

$$E^{\hat{r}} = \left\{ \frac{15\omega r^3}{16M^5 c} \left\{ C_3 \left[\left(3 - \frac{2r}{M} \right) \ln N^2 + \frac{2M^2}{3r^2} + \frac{2M}{r} - 4 \right] + \frac{2M^2}{5r^2} \ln N^2 + \frac{4M^3}{5r^3} \right\} \right.$$
$$\left. + \frac{\Omega}{6cR^2} C_1 C_2 \left[\left(3 - \frac{2r}{M} \right) \ln N^2 + \frac{2M^2}{3r^2} + \frac{2M}{r} - 4 \right] \right\} \left[\cos\chi (3\cos^2\theta - 1) + 3\sin\chi\cos\lambda\sin\theta\cos\theta \right] \mu \,, \tag{87}$$

$$E^{\hat{\theta}} = -\left\{ \frac{45\omega r^3}{16M^5 c} N \left\{ C_3 \left[\left(1 - \frac{r}{M} \right) \ln N^2 - 2 - \frac{2M^2}{3r^2 N^2} \right] + \frac{4M^4}{15r^4 N^2} \right\} \right.$$
$$\left. + \frac{\Omega}{2cR^2} C_1 C_2 N \left[\left(1 - \frac{r}{M} \right) \ln N^2 - 2 - \frac{2M^2}{3r^2 N^2} \right] \right\} \left[2\cos\chi\sin\theta\cos\theta - \left(\cos^2\theta - \sin^2\theta \right) \sin\chi\cos\lambda \right] \mu$$
$$+ \frac{3(\Omega - \omega) r}{8M^3 cN} \left[\ln N^2 + \frac{2M}{r} \left(1 + \frac{M}{r} \right) \right] (\sin\chi\cos\lambda)\mu \,, \tag{88}$$

$$E^{\hat{\phi}} = -\left\{ \frac{45\omega r^3}{16M^5 c} N \left\{ C_3 \left[\left(1 - \frac{r}{M} \right) \ln N^2 - 2 - \frac{2M^2}{3r^2 N^2} \right] + \frac{4M^4}{15r^4 N^2} \right\} + \frac{\Omega}{2cR^2} C_1 C_2 N \left[\left(1 - \frac{r}{M} \right) \ln N^2 - 2 - \frac{2M^2}{3r^2 N^2} \right] \right.$$
$$\left. - \frac{3(\Omega - \omega) r}{8M^3 cN} \left[\ln N^2 + \frac{2M}{r} \left(1 + \frac{M}{r} \right) \right] \right\} (\sin\chi\cos\theta\sin\lambda)\mu \,. \tag{89}$$

where $N^2 \equiv 1 - 2M/R$, and C_1, C_2, C_3 are determined through boundary conditions.

Features of solutions (87)–(89) that should be noticed are

- the MFs are amplified in strength but have the same structure as in flat spacetime; higher-order terms in Ω are necessary to introduce rotational corrections;
- the dragging of reference frames introduces a contribution $\mathcal{O}(\omega)$ to the EF, which does not have a flat spacetime analogue. This effect is present already at $\mathcal{O}(\Omega)$;

7.3 Rotating Magnetized Conductor in a Schwarzschild Spacetime: Exterior Solution in the Wave-Zone

I now consider the the solution of the Maxwell equations outside the light cylinder (i.e. in the wave-zone) produced by a perfectly conducting magnetic dipole rotating in vacuum. For simplicity and because the rotation-induced corrections are very small at these distances, I will consider a spherical spacetime and the equivalent of the ZAMO observers.

The simplest approach to the problem is to express the EMFs in the wave-zone through

two scalar functions U and V, whose angular dependence is expanded in spherical harmonics and have a harmonic time dependence (Bouwkamp & Casimir, 1954)

$$U(t,r,\theta,\phi) \equiv rU_{\ell m}(r)Y_{\ell m}(\theta,\phi)e^{-i\omega t}\ , \qquad V(t,r,\theta,\phi) \equiv rV_{\ell m}(r)Y_{\ell m}(\theta,\phi)e^{-i\omega t}\ . \quad (90)$$

In the wave-zone these scalar functions will be solutions of a wave equation and can be expressed in terms of outgoing spherical Hankel functions $H_\ell(\omega r)$ in the form

$$U_{\ell m}(r) = \left[\ell\left(\ell+1\right)\right]^{1/2} H_\ell(\omega r)u_{\ell m}\ , \qquad V_{\ell m}(r) = -\left[\ell\left(\ell+1\right)\right]^{1/2} H_\ell(\omega r)v_{\ell m}\ , \quad (91)$$

where $v_{\ell m}, v_{\ell m}$ are determined from boundary conditions on the stellar surface. The components of the EMFs in the wave-zone assume then the form (Rezzolla & Ahmedov, 2004)

$$B^{\hat{r}} = \frac{1}{r} U_{\ell m} Y_{\ell m} e^{-i\omega t} = -i \frac{\Omega_{_R} R^3}{N_{_R} r^2} f_{_R} B_0 \sin\chi \sin\theta e^{i[\Omega(r-t)+\phi]} \,, \tag{92}$$

$$B^{\hat{\theta}} = \frac{1}{r\ell\left(\ell+1\right)} \left[\partial_r \left(r U_{\ell m} \right) \partial_\theta Y_{\ell m} - \frac{i\omega}{\sin\theta} r V_{\ell m} \partial_\phi Y_{\ell m} \right] e^{-i\omega t} = \frac{1}{2} \frac{\Omega_{_R}^2 R^3}{r} f_{_R} B_0 \sin\chi \cos\theta e^{i[\Omega(r-t)+\phi]} \,, \tag{93}$$

$$B^{\hat{\phi}} = \frac{1}{r\ell\left(\ell+1\right)} \left[\partial_r \left(r U_{\ell m} \right) \frac{1}{\sin\theta} \partial_\phi Y_{\ell m} + i\omega r V_{\ell m} \partial_\theta Y_{\ell m} \right] e^{-i\omega t} = \frac{i}{2} \frac{\Omega_{_R}^2 R^3}{r} f_{_R} B_0 \sin\chi e^{i[\Omega(r-t)+\phi]} \,, \tag{94}$$

and

$$E^{\hat{r}} = \frac{1}{r} V_{\ell m} Y_{\ell m} e^{-i\omega t} = 0 \,, \tag{95}$$

$$E^{\hat{\theta}} = \frac{1}{r\ell\left(\ell+1\right)} \left[\partial_r \left(r V_{\ell m} \right) \partial_\theta Y_{\ell m} + \frac{i\omega}{\sin\theta} r U_{\ell m} \partial_\phi Y_{\ell m} \right] e^{-i\omega t} = E_0 \sin\chi e^{i[\Omega(r-t)+\phi]} = B^{\hat{\phi}} \,, \tag{96}$$

$$E^{\hat{\phi}} = \frac{1}{r\ell\left(\ell+1\right)} \left[\partial_r \left(r V_{\ell m} \right) \frac{1}{\sin\theta} \partial_\phi Y_{\ell m} - i\omega r U_{\ell m} \partial_\theta Y_{\ell m} \right] e^{-i\omega t} = E_0 \sin\chi \cos\theta e^{i[\Omega(r-t)+\phi]} = -B^{\hat{\theta}} \,. \tag{97}$$

where the last expression for each field component are specialized to $\ell = 1$ (see Rezzolla & Ahmedov 2004 for the $\ell = 2$ terms) and are to be taken in their real part only. Note how the EMFs behave as radially outgoing waves for which $|B^{\hat{r}}/B^{\hat{\theta}}| \sim |B^{\hat{r}}/B^{\hat{\phi}}| \sim 1/\Omega r \ll 1$.

Using these results we can estimate the luminosity of the dipolar EM radiation L_{em} in

terms of the integral of the Poynting vector $\mathbf{P}$

$$L_{em} \equiv \int_{\partial\Sigma} P^{\hat{r}} dS = \frac{1}{4\pi} \int_{\partial\Sigma} (\mathbf{E} \times \mathbf{B})^{\hat{r}} \, dS \, , \tag{98}$$

where the integral is made over the 2-sphere $\partial\Sigma$ of radius $r \gg 1/\Omega$.

Substituting in (98) the expressions for the EMFs in the wave-zone, the power (98) radiated in the form of dipolar electromagnetic radiation is then

$$L_{em} = \frac{1}{8\pi} \left(|u_{\ell m}|^2 + |v_{\ell m}|^2 \right) = \frac{|u_{11}|^2}{8\pi} = \frac{\Omega_{_R}^4 R^6 (f_{_R} B_0)^2}{6c^3} \sin^2 \chi \, . \tag{99}$$

where $\Omega_{_R} \equiv \Omega(r = R)$ and $f_{_R} = f_{_R}(M, R)$ represents the general relativistic *amplification* of the MF strength. A comparison with the equivalent Newtonian expression (Pacini 1968)

$$(L_{em})_{\rm Newt.} = \frac{\Omega^4 R^6 B_0^2}{6c^3} \sin^2 \chi \, , \tag{100}$$

shows that the general relativistic corrections in (99) are due partly to the MF amplification and partly to the increase in the effective rotational angular velocity produced by the

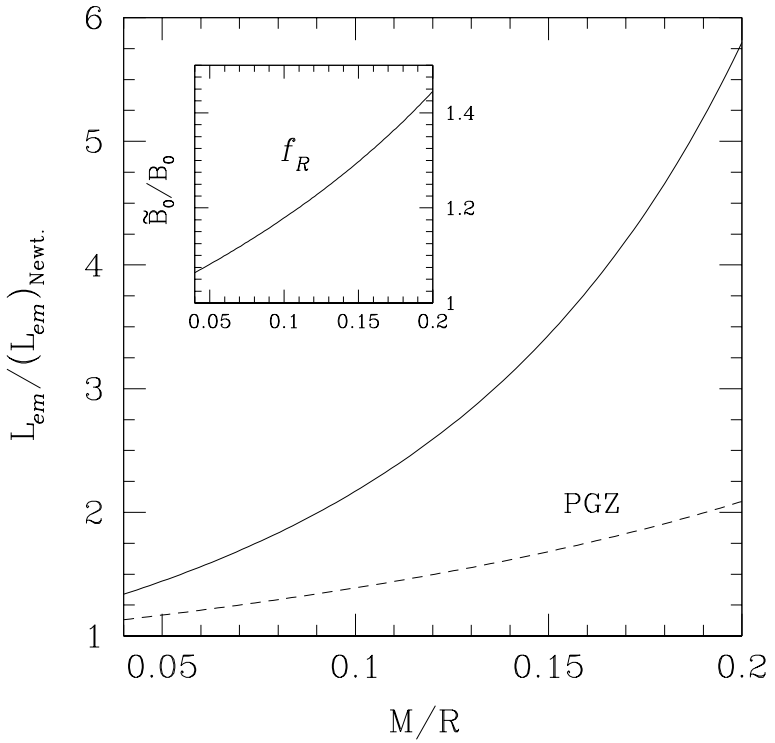

Figure 12: General relativistic amplification of the dipolar energy loss as a function of the compactness, the dashed being the heuristic estimate by Geppert et al., 2000. The inset shows the MF amplification produced by the spacetime curvature.

gravitational redshift [*i.e.* $\Omega = \Omega_{_R} N_{_R}$]. Overall, therefore, the presence of a curved spacetime has the effect of increasing the rate of EM radiation energy loss by an amount

$$\frac{L_{em}}{(L_{em})_{\rm Newt.}} = \left(\frac{f_{_R}}{N_{_R}^2}\right)^2 \ . \tag{101}$$

This is a factor between 2 and 6 in the typical range for the compactness of relativistic stars and the dependence is shown in Fig. 12 with a solid line (the dashed line refers to a heuristic estimate by Geppert et al., 2000).

The expression for the energy loss (99) can also be used to determine the spin-evolution of a pulsar that is converting its rotational energy into electromagnetic radiation. Relating the EM energy loss L_{em} to the loss of rotational kinetic energy $E_{\rm rot}$ defined as

$$E_{\rm rot} \equiv \frac{1}{2}\int d^3\mathbf{x}\sqrt{\gamma}e^{-\Phi(r)}\rho(\delta v^{\hat{\phi}})^2 \,, \tag{102}$$

and introducing the general relativistic moment of the inertia of the star

$$\widetilde{I} \equiv \int d^3\mathbf{x}\sqrt{\gamma}e^{-\Phi(r)}\rho r^2\sin^2\theta \,, \tag{103}$$

whose Newtonian limit gives the well-known expression for a spherical distribution of

matter $I \equiv (\widetilde{I})_{\rm Newt.} = \frac{2}{5} M R^2$, the energy budget is then readily written as

$$\dot{E}_{\rm rot} \equiv \frac{d}{dt}\left(\frac{1}{2}\widetilde{I}\Omega^2\right) = -L_{em}\ . \tag{104}$$

Of course, in enforcing the balance (104) we are implicitly assuming all the other losses of energy (*e.g.* those to GWs) to be negligible. This can be a reasonable approximation except during the initial stages of the pulsar's life, during which the energy losses due to emission of gravitational radiation will dominate because of the steeper dependence on the angular velocity (*i.e.* $\dot{E}_{\rm GW} \propto \Omega^6$).

Expression (104) can also be written in a more useful form in terms of the pulsar's most important observables: the period P and its time derivative $\dot{P} \equiv dP/dt$. In this case, in fact, using expression (99) and (104), it is not difficult to show that

$$P\dot{P} = \left(\frac{2\pi^2}{3c^3}\right)\frac{1}{N_R^4}\frac{R^6\widetilde{B}_0^2}{\widetilde{I}} = \left(\frac{f_R^2}{N_R^4}\frac{I}{\widetilde{I}}\right)(P\dot{P})_{\rm Newt.}\ , \tag{105}$$

where the Newtonian expression is given by (Gunn & Ostriker 1969)

$$(P\dot{P})_{\rm Newt.} \equiv \left(\frac{2\pi^2}{3c^3}\right)\frac{R^6 B_0^2}{I}\ . \tag{106}$$

Also in this case, general relativistic corrections are introduced through the amplification of the MF, of the stellar angular velocity, and of the stellar moment of inertia (*i.e.* $I/\widetilde{I}$).

8 Gravitational Radiation from Magnetized NSs

If the star is rotating with angular velocity $\mathbf{\Omega}_{\rm rot}$, it will be flattened by centrifugal forces and may also deviate from axisymmetry as a result of shear forces produced either by crystalline or magnetic stresses. Because of this, it is useful to introduce a reference frame, the *asymptotic corotating frame* whose spatial basis vectors $\mathbf{e}_{x'}, \mathbf{e}_{y'}, \mathbf{e}_{z'}$ are along the principal axes of the star (cf. Fig. 13), so that the quadrupole moment in this frame will take the form

$$\mathbf{\mathcal{I}} \equiv \varepsilon_{\rm p} I [\mathbf{e}_{z'} \otimes \mathbf{e}_{z'} - \frac{1}{2}(\mathbf{e}_{x'} \otimes \mathbf{e}_{x'} + \mathbf{e}_{y'} \otimes \mathbf{e}_{y'})] + \frac{1}{2}\varepsilon_{\rm e} I (\mathbf{e}_{x'} \otimes \mathbf{e}_{x'} - \mathbf{e}_{y'} \otimes \mathbf{e}_{y'}), \qquad (107)$$

where $\varepsilon_{\rm p}$ is the stellar *poloidal gravitational oblateness* and $\varepsilon_{\rm e}$ the stellar *equatorial gravitational oblateness*, defined respectively as

$$\varepsilon_{\rm p} I \equiv \mathcal{I}_{z'z'}, \qquad \varepsilon_{\rm e} I \equiv \mathcal{I}_{x'x'} - \mathcal{I}_{y'y'}, \qquad (108)$$

where, in general, $\varepsilon_{\rm e} \ll \varepsilon_{\rm p} \ll 1$.

Furthermore, the star, just like the earth or the sun, is also likely to precess with angular velocity $\mathbf{\Omega}_{\rm prec} = \Omega_{\rm prec}\mathbf{e}_{z'}$, so that the *total angular velocity* will be

$$\mathbf{\Omega} = \mathbf{\Omega}_{\rm rot} + \mathbf{\Omega}_{\rm prec}, \qquad \text{and} \qquad \mathbf{\Omega} = \Omega\mathbf{e}_z. \tag{109}$$

is a constant of motion in the asymptotic inertial frame.

As seen in the corotating frame, the angular velocity of rotation $\mathbf{\Omega}_{\rm rot}$ will precess at a constant rate $\Omega_{\rm prec}$ around the near axisymmetry axis $\mathbf{e}_{z'}$ keeping the angle to that that axis $\theta_{\rm w} \equiv \cos^{-1}(\mathbf{\Omega}_{\rm rot}\cdot\mathbf{e}_{z'}) = \text{const.}$ constant in time. The angle $\theta_{\rm w}$ is referred to as the *"wobble angle"*. A schematic description of the two asymptotic frames is shown in Fig. 13 where are indicated the different orientations of angular velocity vectors $\mathbf{\Omega}, \mathbf{\Omega}_{\rm rot}$, and $\mathbf{\Omega}_{\rm prec}$.

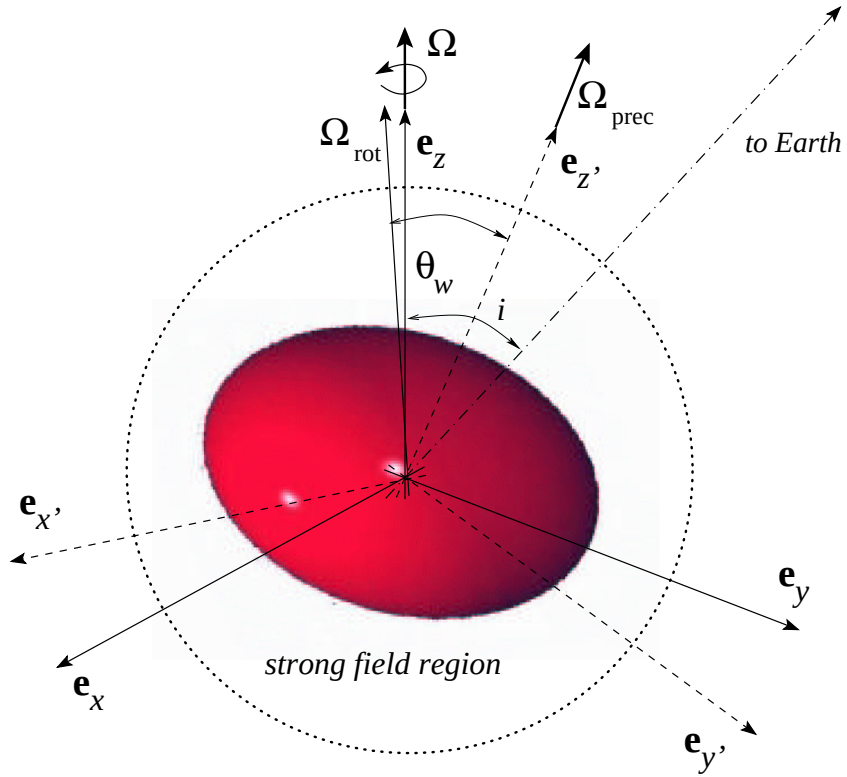

Figure 13: Schematic view of a rotating NS and of the relevant reference frames: the *asymptotic inertial frame* (basis vectors $\mathbf{e}_i$) and the *asymptotic corotating frame* (basis vectors $\mathbf{e}_{i'}$). Note that in general $\mathbf{\Omega} = \mathbf{\Omega}_{\rm rot} + \mathbf{\Omega}_{\rm prec}$, although in practice $\mathbf{\Omega} \approx \mathbf{\Omega}_{\rm rot}$.

Note that because of the large degree of axisymmetry expected in NSs, the wobble angle is in general very small $\theta_{\rm w} \ll 1$ and that since $\mathbf{\Omega} = \mathbf{\Omega}_{\rm rot} + \mathbf{\Omega}_{\rm prec}$, not $\mathbf{\Omega}_{\rm rot}$, nor $\mathbf{\Omega}_{\rm prec}$ will be

aligned with $\mathbf{e}_z$ and that small angles will exist between these three vectors. In particular, since

$$\frac{\theta_0}{\theta_{\rm w}} = \frac{(\text{angle between } \mathbf{\Omega}_{\rm rot} \text{ and } \mathbf{e}_z)}{(\text{angle between } \mathbf{\Omega}_{\rm rot} \text{ and } \mathbf{e}_{z'})} = \frac{\Omega_{\rm prec}}{\Omega_{\rm rot}} \sim 10^{-5} - 10^{-8} \ll 1. \tag{110}$$

Within a Newtonian quadrupole approximation (the one we will assume hereafter[4]), the GW emission can be calculated by computing the time variations of the stellar mass quadrupole defined as

$$\mathcal{I}_{jk} \equiv \int \rho(x^j x^k - \frac{1}{3} r^2 \delta_{jk}) d^3x = -I_{jk} + \frac{1}{3} I_i{}^i \delta_{jk}, \tag{111}$$

where I_{jk} is the stellar moment of inertia.

$$I_{jk} \equiv \int \rho(r^2 \delta_{jk} - x^j x^k) d^3x. \tag{112}$$

The problem is therefore quite simple: given the asymptotic inertial frame (the one in

[4]Clearly, this is an approximation but given the uncertainties in the stellar structure and thus in the calculations of the mass quadrupole, it is not the worse one.

which the detector is placed), calculate (111) and its time variations. Omitting the details of the calculation and assuming a proper orientation of the wave polarization axes, the two polarisations will have amplitudes (Zimmermann & Szedenits, Thorne 1988)

$$h_+ = \frac{2}{r}\frac{d^2\mathcal{I}_{\bar{x}\bar{x}}}{dt^2} = -\frac{2}{r}\frac{d^2\mathcal{I}_{\bar{y}\bar{y}}}{dt^2}, \qquad h_\times = \frac{2}{r}\frac{d^2\mathcal{I}_{\bar{x}\bar{y}}}{dt^2}, \tag{113}$$

so that

$$h_+ = \frac{2(1+\cos^2 i)}{r}\varepsilon_{\rm e} I \Omega_{\rm rot}^2 \cos(2\Omega_{\rm rot} t) + \frac{2\sin 2i}{r}\varepsilon_{\rm p} I \theta_{\rm w} \Omega_{\rm rot}^2 \cos[(\Omega_{\rm rot} + \Omega_{\rm prec})t], \tag{114}$$

$$h_\times = \frac{4\cos i}{r}\varepsilon_{\rm e} I \Omega_{\rm rot}^2 \sin(2\Omega_{\rm rot} t) + \frac{4\sin i}{r}\varepsilon_{\rm p} I \theta_{\rm w} \Omega_{\rm rot}^2 \sin[(\Omega_{\rm rot} + \Omega_{\rm prec})t], \tag{115}$$

Note how expressions (114)–(115) separate the contributions coming from the equatorial oblateness and oscillating at $2\Omega_{\rm rot}$ from its sideband contribution coming from the poloidal oblateness and oscillating at $\Omega_{\rm rot} + \Omega_{\rm prec}$. Expressing now the amplitude in terms of the

characteristic amplitudes we obtain

$$h_{c1} = 8\pi^2\sqrt{\frac{2}{15}}\frac{\theta_{\rm w}\varepsilon_{\rm p}I(2f_1)^2}{r} \simeq 7.7\times10^{-20}\theta_{\rm w}\varepsilon_{\rm p}\left(\frac{I}{10^{45}\ {\rm g\ cm^2}}\right)\left(\frac{2f_1}{1\ {\rm kHz}}\right)^2\left(\frac{10\ {\rm kpc}}{r}\right), \quad (116)$$

$$h_{c2} = 8\pi^2\sqrt{\frac{2}{15}}\frac{\varepsilon_{\rm e}I f_2^2}{r} \simeq 7.7\times10^{-20}\varepsilon_{\rm e}\left(\frac{I}{10^{45}\ {\rm g\ cm^2}}\right)\left(\frac{f_2}{1\ {\rm kHz}}\right)^2\left(\frac{10\ {\rm kpc}}{r}\right), \quad (117)$$

where $f_1 \equiv (\Omega_{\rm rot}+\Omega_{\rm prec})/2\pi$ and $f_2 \equiv \Omega_{\rm rot}/\pi \simeq 2f_1$ is the high-frequency part of the signal. Note that since $h_c \propto \varepsilon_{\rm e,p}$ and $h_c \propto (f_{1,2})^2$, the best sources of GWs are highly distorted and highly spinning NSs.

The rates of energy-loss to GWs corresponding to the amplitudes (116)–(117) are not difficult to calculate and will depend on a further time derivative of the mass quadrupole

$$\frac{dE_{\rm GW}}{dt} = \frac{1}{5}\frac{G}{c^5}\left\langle\frac{d^3\mathcal{I}_{\bar{j}\bar{k}}}{dt^3}\frac{d^3\mathcal{I}_{\bar{j}\bar{k}}}{dt^3}\right\rangle^2, \quad (118)$$

yielding in this case

$$\left(\frac{dE_{\rm GW}}{dt}\right)_1 = \frac{8}{5}\frac{G}{c^5}(2\pi f_1)^6(\theta_{\rm w}\varepsilon_{\rm p}I)^2 = \frac{3}{4}\frac{G}{c^5}(\pi f_1 r)^2 h_{c1}^2, \tag{119}$$

$$\left(\frac{dE_{\rm GW}}{dt}\right)_2 = \frac{32}{5}\frac{G}{c^5}(\pi f_2)^6(\varepsilon_{\rm p}I)^2 = \frac{3}{4}\frac{G}{c^5}(\pi f_2 r)^2 h_{c2}^2. \tag{120}$$

Note the steeper dependence on the spin frequency, i.e. $\dot{E}_{\rm GW} \propto \Omega^6$, to be contrasted with the corresponding energy-loss rates for the emission of EM radiation, $\dot{E}_{\rm EM} \propto \Omega^4$ [cf. eqs. (99)–(100)].

In analogy to what done for a pulsar being spun-down by dipolar EM radiation and after defining the decay timescale $T_{\rm GW} \equiv (\Omega/\dot{\Omega})_0$, we can calculate a braking index $n = 5$ and the time evolution of spin frequency produced by GW losses to be

$$\Omega(t) = \Omega_{\rm i}\left(1 + \frac{4\Omega_{\rm i}^4}{\Omega_0^4}\frac{t}{T_{\rm GW}}\right)^{-1/2}. \tag{121}$$

8.1 Magnetic Stresses

Magnetic stresses in a pulsar together with the shear stresses of the stellar parts that are in a crystalline form (i.e. the crust) are the only forces that can prevent the star to be axisymmetric about its rotation axis: i.e. that can produce a wobble angle $\theta_{\rm w}$ and an equatorial oblateness $\varepsilon_{\rm e}$. In particular, in the highly conducting matter composing NSs, in fact, the magnetic field will introduce a magnetic pressure $p_{\rm mag}$ orthogonal to the field lines and a magnetic tension $-p_{\rm mag}$ along the field lines.

However, in NSs the competition with the other forces is very difficult since the Coulomb interaction which is the source of shear tensor T^S_{jk} or of the magnetic force, is much weaker that the degeneracy effects and the nuclear interaction which are the sources of the isotropic pressure force p, and also far weaker that the gravitational interaction and centrifugal

forces (the latter responsible for $\varepsilon_{\rm p}$). Yet, detectable deformations can be produced if the MFs are sufficiently intense and while precise estimates will depend on a number of details such as intensity of the MF, its location, its lifetime, etc, with dimensional arguments we can state that the magnetic force will be

$$F_{\rm mag} \sim \frac{p_{\rm mag}}{R} \sim \frac{B^2/8\pi}{R} \lesssim F_{\rm cent}, \tag{122}$$

where $F_{\rm cent}$ is centrifugal force

$$F_{\rm cent} \sim \Omega_{\rm rot}^2 R\rho \lesssim F_{\rm grav}. \tag{123}$$

which contrasts the gravitational and pressure forces to produce the spheroidal oblateness

$$\varepsilon_{\rm p} \sim \frac{F_{\rm cent}}{F_{\rm grav}} \sim \frac{(\Omega_{\rm rot}R)^2}{M/R} \sim \left(\frac{0.5\ {\rm msec}}{P_{\rm rot}}\right)^2 \sim 10^{-2} - 10^{-4}. \tag{124}$$

As a result, the magnetically-induced equatorial oblateness will be

$$(\varepsilon_{\rm e})_{\rm mag} \sim \theta_{\rm w}\varepsilon_{\rm p} \sim \frac{I_c}{I}\frac{F_{\rm mag}}{F_{\rm grav}} \sim \frac{I_c}{I}\frac{p_{\rm mag}}{p} \sim 10^{-8}\left(\frac{B_{\rm crust}}{10^{12}\ {\rm G}}\right)^2 . \tag{125}$$

where $I_c \simeq 10^{-3} I$ is the crust's contribution to the moment of inertia I, and $B_{\rm crust}$ is the MF in the crust and which is expected to be close to the measured surface one of $\sim 10^{12}$ G.

9 MF Evolution in Rotating and Cooling NSs

The calculation of the evolution of the thermal, magnetic and rotational properties of a NS is clearly a complex problem in which a number of important factors need to be considered simultaneously and with the same accuracy. In the case of *isolated* rotating NSs, in fact, the system will generically loose its rotational energy to the emission of EM or gravitational radiation. Both of them depend on the properties of the MF and its time evolution which, however, depends on the thermal history of the star. First attempts to investigate systematically the rotational evolution of magnetized NSs with predominant dipolar magnetic field anchored in the crust can be found in Page et al. (2000) for the case of isolated stars and in Lavagetto et al. (2004) when the NS is present in a binary system.

References

[1] Anderson, J. L., Cohen, J. M., 1970, Astrophys. Space Science, 9, 146

[2] Bardeen, J. M., Press, W. H., Teukolsky, S. A., 1972. ApJ, 178, 347.

[3] Bonanno A., Rezzolla L., Urpin V., 2003 A&A, 410 L33

[4] Bruenn S., Dineva T. 1996, ApJ, 458, L71

[5] Bruenn S., Mezzacappa A. 1994, ApJ, 433, L45

[6] Burrows A., Lattimer J. 1986, ApJ 307, 178

[7] Chandrasekhar S., 1970, Phys. Rev. Letters 24, 611

[8] Deutsch, A. J., 1955, Ann. Astrophys., 1, 1

[9] Duncan, R. C., Thompson, C., 1992, ApJ, 392, L9.

[10] Epstein R. 1979, MNRAS, 188, 305

[11] Friedman J. L., Schutz B. F., 1978, ApJ 221, 937; 1978 222, 281

[12] Geppert, U., Page, D., Zannias, T., 2000, Phys. Rev. D, 61, 123004

[13] Ginzburg, V. L., Ozernoy, L. M., 1964, Zh. Eksp. Teor. Fiz., 47, 1030

[14] Gold, T., 1968 Nature 218, 731

[15] Goldreich, P., Julian, W. H., 1969. ApJ, 157, 869.

[16] Gunn, E.J., Ostriker, J.P., 1969, Nature, 221, 454; 1969, ApJ, 157, 1395

[17] Hartle, J. B., Thorne, K. S., 1968. ApJ, 153, 807.

[18] Hewish, A., Bell, S. J, Pilkington, J. D. H., Scott, P. F., Collins, R. A., 1968 Nature 217, 709

[19] Keil W., Janka H.-T. 1995, A&A, 296, 145

[20] Keil W., Janka H.-T., Müllerr E. 1996, ApJ, 473, L111

[21] Landau, L.D., Lifshitz, E.M., 1987, The Classical Theory of Fields, 4th ed., Pergamon Press, Oxford

[22] Lavagetto, G., Burderi, L., D'Antona, F., Di Salvo, T., Iaria, R., Robba, N. R., 2004, MNRAS, 348, 73

[23] Lighthill J. , *Waves in Fluids*, Cambridge Univ. Press, Cambridge, UK 1980, p. 279.

[24] Levin Y., Ushomirsky G., 2001, MNRAS, MNRAS 324, 917L

[25] Lindblom L., Tohline J. E., Vallisneri M., 2001 Phys. Rev. Lett. 86, 1152-1155

[26] Livio M., Buchler J., Colgate S. 1980, ApJ, 238, L139

[27] Miralles J., Pons J., Urpin V. 2000, ApJ, 543, 1001

[28] Miralles J., Pons J., Urpin V. 2002, ApJ, 574, 356

[29] Misner C. W., Thorne K. S., Wheeler J. A., 1974, *"Gravitation"*, Freeman, NY

[30] Moffatt, H. K., 1978, *Magnetic Field Generation in Electrically Conducting Fluids*, Cambridge Univ. Press, Cambridge, UK

[31] Muslimov, A., Harding, A. K., 1997, ApJ, 485, 735.

[32] Muslimov, A., Tsygan, A. I., 1992, MNRAS, 255, 61.

[33] Narayan R. 1987, ApJ, 319, 162

[34] Pacini, F., 1968, Nature, 219, 145

[35] Parker E. N., 1979, *Cosmical Magnetic Fields*, Clarendon Press, Oxford, UK § 4.3.

[36] Petterson, J. A., 1974. Phys. Rev. D 10, 3166

[37] Owen B. J., Lindblom L., Cutler C., Schutz B. F., Vecchio A., N. Andersson, 1998, Phys. Rev. D 58, 084020

[38] Page, D., Geppert, U., Zannias, T., 2000, A&A 360, 1052

[39] Pavlov G., Zavlin V., Sanwal D., Trümper J. 2002, ApJ, 569, L95

[40] Pons J., Reddy S., Prakash M., Lattimer J., Miralles J. 1999, ApJ, 513, 780

[41] Potekhin A. Y., Baiko D. A., Haensel P., Yakovlev D. G., 1999, A&A 346, 345

[42] Rampp M., Janka H.-T. 2000, ApJ, 539, L33

[43] Rezzolla L., Lamb F. K., and Shapiro S. L., 2000, ApJ 531, L141

[44] Rezzolla L., Lamb F. K., Marković D., Shapiro S. L., 2001 Phys. Rev. D, 64, 104013; Phys. Rev. D, 64, 104014 (2001)

[45] Rezzolla, L., Ahmedov, B.J., Miller, J.C., 2001a, MNRAS, 322, 723; 338, 816 (2003)

[46] Rezzolla, L., Ahmedov, B.J., Miller, J.C., 2001b, Found. of Phys., 31, 1051

[47] Rezzolla, L., Ahmedov, B.J., 2004, 352, 1161

[48] Rüdiger G., Kitchatinov L. 1993. A&A, 269, 581

[49] Sá P. M., 2004, Phys.Rev. D69 084001

[50] Salgado M., Bonazzola S., Gourgoulhon E., Haensel P., 1994a, A&A 291, 155

[51] Sanwal D., Pavlov G., Zavlin V., Teter M. 2002, ApJ, 574, L61

[52] Shapiro S. L., Teukolsky S. A., *"Black Holes, White Dwarfs and Neutron Stars "*, J. Wiley NY (1984)

[53] Stergioulas N., Font J. A., 2001, Phys. Rev. Lett. 86, 1148

[54] Thompson C., Duncan R. 1993, ApJ, 408, 194

[55] K. S. Thorne, 1988, *Lecture Notes* Caltech, Pasadena, USA

[56] Wasserman, I., Shapiro, S. L., 1983, ApJ, 265, 1036.

[57] Xu R.X., Busse F.H. 2001, A&A, 371, 963

[58] Zanotti, O., Rezzolla, L., 2002, MNRAS, 331, 376

[59] Zimmermann M., Szedenits E., 1979, Phys. Rev. D 20, 351